POLITECNICO MILANO 1863

SCUOLA DI INGEGNERIA INDUSTRIALE E DELL'INFORMAZIONE

Extracting periodic signals from machine direction product quality variation

Tesi di Laurea Magistrale in
Mechanical Engineering - Ingegneria Meccanica

Author: **Carlotta Massotti**

Student ID: 968966
Advisor: Prof. Marco Tarabini
Co-advisors: Assistant Prof. Raine Viitala
Academic Year: 2021-22

Abstract

Non-idealities and vibrations of rolls cause periodical variation of paper quality parameters during the production process. The frequency of the variation is strictly related to the rotational frequency of the rotating components. This thesis investigates the application of an optimal filter as a method to estimate the impact of rotating components of a paper machine on the quality of the final product. The proposed method is a suitable procedure to extract periodic patterns from a noisy mixture, i.e., a signal composed of different harmonic series and noise, and presents some advantages over the classical usage of the Fourier transform. To verify the possibility of using the method as a monitoring tool for paper quality, tests are first performed on an artificially generated signal and finally on data measured on a strip of cardboard. The artificially generated signal was built to reproduce a signal of caliper variation measured in the laboratory on a strip of cardboard. When applied to a synthetic signal composed of 9 harmonic series with a signal to noise ratio close to 1.5, the filter returned a maximum average error of 0.014 µm in the amplitude values of the harmonic components of the extracted series. Moreover, the filter showed a comparable result with the software currently used in laboratory analysis. The software detects the frequencies of the machine components that are causing a high quality variation. The result obtained with the filter can be considered even more accurate. Indeed, the difference between the frequency extracted by the software and that of the machine component was 0.074 Hz, whereas it was only 0.006 Hz with the optimal filter.

Keywords: Optimal filter, machine direction, paper machine, roll

Abstract in lingua italiana

I componenti rotanti di una macchina adibita alla produzione di carta hanno un elevato impatto sulla qualità del prodotto finale. Le non idealità e le vibrazioni dei rulli causano variazioni periodiche dei parametri di qualità della carta, con una frequenza che è strettamente correlata alla frequenza di rotazione dei componenti. In questa tesi un filtro ottimo viene proposto come metodo per stimare l'impatto dei componenti rotanti di un impianto di produzione sulla qualità del prodotto finale. Il metodo proposto è in grado di estrarre segnali periodici da un segnale contenente più serie di armoniche e rumore e presenta alcuni vantaggi rispetto all'uso classico della trasformata di Fourier. Per verificare la possibilità di utilizzare il metodo come strumento di monitoraggio della qualità della carta, sono stati eseguite delle prove prima su un segnale generato artificialmente e infine su dati misurati su un campione di cartone. Il segnale sintetico è stato generato in modo da riprodurre la variazione di spessore misurata in laboratorio su un campione di cartone. Il filtro, applicato a un segnale sintetico composto da 9 serie di armoniche con un rapporto segnale rumore prossimo a 1.5, ha restituito un errore medio di 0,014 µm nei valori di ampiezza delle componenti armoniche della serie estratta. Il metodo ha inoltre mostrato un risultato comparabile con quello di un software attualmente utilizzato nelle analisi di laboratorio. Il software individua le frequenze dei componenti della macchina che causano un'elevata variazione di qualità. Il risultato ottenuto con il filtro può essere considerato anche più accurato. Infatti, la differenza tra la frequenza estratta e quella del componente della macchina è uguale a 0,074 Hz quando viene utilizzato il software, mentre è uguale a 0,006 Hz con il filtro ottimo.

Parole chiave: Filtro ottimo, direzione della macchina, macchina per la produzione di carta, rulli

Contents

1 | Introduction

In many production processes, rotating rolls are used to form the final product. This is the case for papermaking, steel and non-ferrous metal manufacturing, and plastic film production. The quality of the final product is subjected to periodic variations, with a periodicity that depends on the rotational frequency of the rolls [24]. The extent of the variation imposed by a single roll is related to its run-out, which is the sum of the central axis movement and the surface roundness profile. Rotors properties must satisfy specific requirements to ensure the final target quality. It is possible to measure rotor characteristics in laboratories, but this implies stopping the production and removing the component from the machine. In-process measurements are, instead, more difficult to carry out and typically it is not possible to obtain comprehensive measurements [5]. A possible way to detect defects or wear in some components of the machine is to continuously measure quality parameters in the end product. Additionally, sensors placed on the machine, measuring for example vibrations or acoustic emissions, can be helpful for the same purpose.

During the last decades, requirements for paper quality have become tighter in manufacturing industries for paper and board production and machine speed has increased, thus requiring higher production efficiency and effectiveness [3]. The increase in production volumes is mainly due to a larger tissue consumption and a higher demand for paper packaging. In fact, in 1993 the global tissue consumption was 15.5 million tonnes, while in 2018 it reached 38.7 million tonnes [1]. The rise of e-commerce and the need for a more sustainable substitute for plastic have instead driven the growth of the production of paper packaging [2]. To reduce production waste, and therefore increase production efficiency, it is fundamental to measure quality variation. Variation is natural since it starts at the source of the raw material, but it can worsen at each step of the manufacturing process [4], therefore it is necessary to keep it under control. Cutshell [4] presented the problem of variation with a statistical approach, showing how limiting the amount of variation can help in decreasing the quality target value of a parameter, reducing the overall cost of production.

Different quality parameters can be measured on the final product and their variation can be categorized in terms of amplitude, frequency, and direction [23]. The main directions in which the paper is examined are machine direction (MD), the direction of the flow of material in the machine, and cross direction (CD), the direction perpendicular to MD (Figure 1.1). Random or residual (R) variation is obtained by subtracting from the total variation MD and CD variation [4].

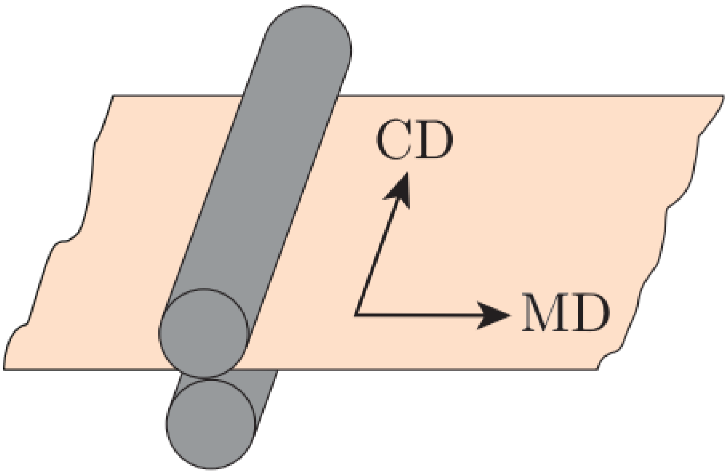

Figure 1.1: Graphical representation of MD and CD [5].

1.1. Research problem

In this thesis, a method to separate the effect of machine components, particularly rolls, on paper parameter variations in MD is analyzed. Rolls are the main components of a paper machine, representing 60% of its entire cost [28].

As stated in previous works [5], it is possible to distinguish periodic components at frequencies very similar to the rotating frequencies of some rolls in the measurement of paper parameters. Defects in this type of machine components manifest themselves in the signals acquired by the sensors positioned on the machine as harmonics with a frequency that is equal to or a multiple of the rotational frequency of the rolls.

Due to limitations in the manufacturing accuracy of rolls and bearings, and error in the mounting procedure undesired vibrations are present in the machine. Unbalance, bending stiffness variation, and roundness error in the cross-section profile of the rotor, for example, cause excitations at a frequency that depends on the type of defect, but in all cases is a multiple of the rotational one. The amplitude of the imposed variation on the product depends on the entity of the defect. Geometrical errors in the bearing elements can, in the same way, cause periodic excitation. Additionally, imperfections in the mounting of the roll on the machine and flexing of the supports can cause end movement vibrations.

If a periodic pattern with a fundamental frequency equal to the rotational frequency of one roll is extracted from the signal, it is possible to estimate the impact of that roll on the final paper quality. The result can be used to monitor the condition of the machine components, prevent faults, and improve quality, acting on the component or section of the machine that is causing the most variations.

In theory, the Discrete Fourier Transform (DFT) can be applied to estimate the spectrum of the signal and to extract the harmonic components. Although it is a very light method from the computational point of view, it presents some limitations. The DFT, indeed, has a frequency resolution limited by the sampling frequency and the length of the signal, i.e., $\Delta f = \frac{f_s}{N}$, and it is not efficient in presence of a high level of noise. In paper machine manufacturing many rotating machine elements have almost identical sizes and rotational speeds and the measurement environment is quite noisy.

This thesis investigates a different approach that overcomes some of the limits of the DFT. One of the main advantages of the selected method is that the frequency to be extracted can be chosen arbitrarily, regardless of sampling frequency and DFT bin spacing.

The frequencies of the rotating components are estimated as the ratio between the machine operating speed and the rotor diameters. Values very similar to the estimated ones have been detected in signals of quality parameter variations in [5] through the hMUSIC algorithm. Once the desired periodic signal has been extracted from the original noisy mixture the impact of the roll can be estimated by computing the root mean square error (RMS) of the output signal. The higher the RMS the higher the effect of that roll on the quality.

The study is mainly concerned with identifying the possible sources of error and limitations of the method to understand if, and in which conditions, it can be a suitable tool to monitor quality in industrial applications. The data available comes from a paper production plant, but the results obtained can be valid every time rotating rolls are used to form the final product, e.g., steel rolling and manufacturing of various plastic films.

1.2. Aim of the study

Currently, many sensors are present on the machine to control the process. Basis weight, for example, is continuously measured, and feedforward and feedback control actions are applied to regulate the stock flow to reduce variations [3]. In addition, condition monitoring is performed thanks to a large number of sensors distributed on the machine. The most important measurements for this maintenance action are vibration measurement, temperature measurement, current analysis of asynchronous motors, wear particle analyses for lubricating and hydraulic oils, and acoustic emission [3]. Moreover, the final quality is supervised with online measurements on the finished product but, currently, there is no procedure to directly relate quality variation to a specific component of the machine. The SOS (separate original signal) analysis of the software developed by Tapio Technologies company can extract periodic components from the acquired signal and correlate them to a specific machine element. Some examples of successful applications of this software are reported in [14]. However, this is a very old method and, additionally, it requires offline measurements, i.e., carried out separately from the process.

This research aims to study and develop a method to analyze signals from online measurements, i.e., performed in-process, extracting from these repeating patterns. This can have different purposes in industrial applications. It is, in fact, useful to understand in which way a machine component contributes to the quality variation, thus correlating this component, or the machine section, to a quality characteristic. Moreover, if data are continuously acquired with online measurements on the machine, quality can be kept under control, setting thresholds, according to the required target values. If a certain parameter overcomes that threshold, it is possible to identify the component which has caused the variation and do the required maintenance. This method also allows monitoring the condition of machine components and planning maintenance operations. Correct and focused maintenance is of fundamental importance to increase the productivity of the plant and avoid waste, thus saving money.

The work consists of a numerical investigation of the method, which is an optimal filter inspired by the principle used in the Amplitude and Phase Estimation (APES) method. The purpose is to study different artificially generated cases that reproduce realistic conditions to understand boundaries for parameters and constraints to be respected to obtain a satisfying result. Investigation of real data is also performed with the final objective of listing the rolls in order of their contribution to the final product and relating sections of the machine to variations in the measured variables.

1.3. Scope of the work

As previously stated, this thesis focuses on the analysis of quality variation caused by rolls in paper production. Other products, such as steel and plastic films, that are manufactured in a similar way are not discussed in this work. However, the method can probably be adapted to be utilized also for these other production processes. Additionally, other sources of variation, e.g., defects in control loops, pulp flow rate variations, or pump malfunctions are not studied. Moreover, only MD is examined, excluding CD variations. In a case in which both CD and MD variations are measured, the complexity of the problem increases, and the two contributions must be separated. One example of the separation problem can be found in [6].

The method for this application has been selected on a theoretical basis, after a literature review of possible methods. The results and the limitations of the method are evaluated, but no practical comparison with other techniques is carried out. The only comparison is made with the result obtained with the SOS analysis of the Tapio analyzer. However, this is done mainly to prove the correctness of the results. The purpose is not to compare the two since the SOS is an offline tool while the proposed method is meant to be used online.

The method is applied to real sets of data. However, the development of the measurement setup and the data acquisition is not part of this thesis work. The optimization of the algorithm execution time is also outside the scope of this work.

1.4. Materials and methods

As anticipated before, an optimal APES filter is chosen among all the possible methods to separate and enhance periodic patterns. The proposed design proved to be efficient for different values of signal to noise ratio (SNR) and signal to interference ratio (SIR) [11].

The filtering algorithm is implemented based on a literature review and with the help of functions already implemented by Christensen. For the implementation, the software *Matlab* is used.

First, an artificially generated signal is studied to evaluate the effectiveness and the limitations of the method. This first step is necessary because the correctness of the result can only be evaluated by giving a completely known signal as input to the filter. There are several assumptions to consider, and the following chapters explain how to deal with these assumptions and in which way, and to what extent it is possible to satisfy them.

Finally, the procedure is also applied to signals coming from the measurement of a real strip of cardboard. Two different sets of data are available:

- Online measurements, acquired with a quality control system (QCS) developed by Valmet

– Offline measurements, obtained with a system developed by Tapio Technologies

In the online measurements, data refer to basis weight, caliper, and moisture, while in the offline measurements only to basis weight and caliper. A final comparison with results obtained with the SOS analysis is also carried out.

1.5. Structure of the thesis

The thesis is organized into 6 chapters. Chapter 2 addresses a review of the literature. Firstly, the paper manufacturing process is briefly explained, and the main sections of a paper machine together with some of the most important paper parameters are described. Next, the chapter presents possible methods to extract periodic patterns. The reasons for the choice of the method, its mathematical implementation, hypothesis, and parameters are also reported. Finally, sources of quality variation are discussed, with a particular focus on the non-idealities of rotating rolls.

Chapter 3 provides all the useful information to understand the results. It describes the set of data available, the Matlab implementation of the filter, and the parameters used. This chapter also explains how the artificial signal is generated, the type of tests performed, and how the performances can be evaluated.

Chapter 4 presents and comments on the results obtained, both with the synthetic signal and with real data while in chapter 5 the results are more deeply discussed. Finally, chapter 6 draws the conclusion of the work, outlining possible future improvements and insights.

2 | Literature review

2.1. Paper manufacturing process

This chapter provides a short explanation of the manufacturing process of paper. This description is not intended to be exhaustive and detailed, but it is meant to provide a general idea of the process. All the information is taken from [3].

At the beginning of the process, raw materials (wood fibers, fillers, adhesives, and chemical additives) are mixed with water, which stimulates the formation of molecular linkages between fibers, forming a stock suspension. The latter is distributed in the headbox, uniformly across the width of the wire, and is then drained in the forming section. This is a crucial step since, here, important structural properties of paper, such as fiber orientation and distribution, are determined. Afterward, the product passes through the press section where it is pressed through several nips, built up by rolls, removing a high amount of water. The moisture level decreases from 80% to 50%. This section of the machine mainly affects paper smoothness and symmetry, fines distribution, linting, moisture, porosity, and bulk. Finally, the product passes to the drying section. Here, external energy is provided through different methods: cylinder contact drying, air drying, and IR drying. The aim is to evaporate water from the web, reaching the target water content. Other sections for finishing operations can be present according to the grade requirements of the end product. Typical operations are winding and reeling but others, such as surface sizing, coating, and calendering can be also carried out. Figure 2.1 shows a paper production plant while figure 2.2 shows a simplified layout of a paper machine, highlighting its main sections.

Moisture level continuously changes along the production line. Moisture is one of the most important parameters in paper production, but many other variables are measured and controlled as well, e.g. basis weight, caliper, ash, gloss, tensile strength, and porosity.

The data in this thesis only refers to basis weight, caliper, and moisture. Basis weight is defined as the mass of one square meter, $[\frac{\mathrm{g}}{\mathrm{m}^2}]$, of paper, or paperboard. It is the most fundamental attribute because a change in this affects most of the other properties,

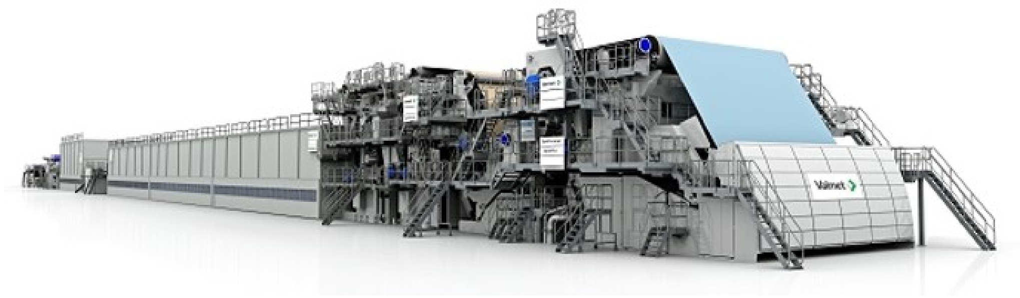

Figure 2.1: Paper machine (downloaded from [34])

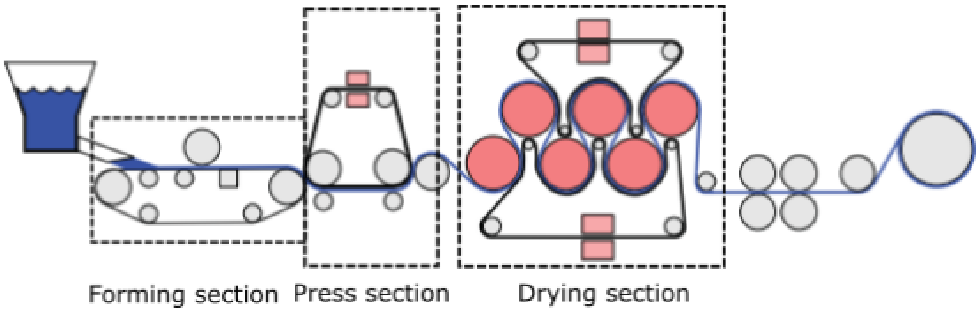

Figure 2.2: Simplified machine layout (modified from [5]).

including strength. It is mainly influenced by the stock flow in the machine, which, for this reason, is strictly controlled. Caliper, instead, is the thickness of the sheet of paper and it is measured in µm. Combined with the basis weight, it returns the stiffness, or bulk, of the product. Moisture is the ratio between the mass of water and the total mass of the product, expressed in percentage.

2.2. Methods to extract periodic patterns

As previously stated, the method applied in this thesis is an optimal APES filter. For the sake of completeness, this chapter provides a short overview of other existing methods to extract periodic patterns, i.e. a source separation problem, describing their advantages and disadvantages.

The problem of source separation is frequently addressed especially in the speech and audio processing field. In the case of blind source separation, non-matrix factorization-based or mask-based methods can be for example applied. In this specific application, the hypothesis of the periodicity of the sources is made, so it is easier to extract each periodic signal once the fundamental frequencies of the sources are known. Several ways to de-noise the signal and extract periodic components from a noisy mixture can be found in the literature.

To accomplish this task, one possibility is to apply a filter. The term filter, technically speaking, refers to a linear, time-invariant filter [7]. Digital filters come in the form of difference equations, which are sums of delayed versions of the input. Each of these delayed versions is scaled by a real number, the filter coefficient [7]. A filter is described by its frequency response function, which, if multiplied by the input, returns the output of the filter. Two traditional filtering methods are, for example, comb filters or sinusoidal filters (also called FFT filters). The classical comb filter is a feedback filter, where a version of the output, delayed by D samples, is added to the input signal. Its impulse response has uniformly spaced sharp peaks, $\frac{2\pi}{D}$ apart in terms of frequency. This comb filter is restricted to integer pitch periods and is rather inefficient [8]. The main restraint of sinusoidal filters is that the frequency resolution is limited by the sampling frequency and the length of the signal. Therefore, sinusoidal filters have some limitations in separating all the rotational frequencies of the rolls.

Harmonic model fitting is another alternative to extract a periodic pattern and it is based on a least-square fitting [18]. The method fails in presence of multiple harmonic series present in the source signal, assuming that there is only one harmonic series corrupted by noise.

Periodic patterns can also be extracted by employing an algebraic method [10]. The advantages of this procedure are a very low computational cost and a short analysis frame. This is due to the separation problem being formulated as a system of linear equations and the required signal length being given by the sum of the number of samples in a period for each harmonic present in the signal. Unlike when applying a filter, the signal will not suffer from distortion [10].

Another possible method that can be used to estimate the amplitude and frequency of a signal is the *energy separation algorithm* [13]. This procedure is based on the estimation of the energy needed by a source to produce the oscillatory signal, which is given by the squared product of the amplitude and frequency of the signal. This method has been proven to be efficient in estimating the time-varying amplitude envelope and instantaneous frequency of a real-valued signal that has both an AM (amplitude modulation) and FM (frequency modulation) structure. Variations of the frequency and amplitude of speech resonances can be modeled and detected at the time scale of one sampling period [13].

2.3. Optimal APES filters

The method analyzed in this thesis is an optimal filter based on the principle of the APES method. The term optimal filtering traditionally refers to a class of methods that can be used for estimating the state of a time-varying system, indirectly observed through noisy measurements [22].

More in detail, the selected type of filter is optimal in a mathematical sense since it minimizes the mean square error between the filter output and the desired output under the constraint that the filter should pass the content at specific frequencies undistorted. The chosen filter is specifically designed for periodic signals. The desired output, in fact, is defined as a sum of sinusoids, with frequencies multiple of a fundamental frequency. This last point makes it suitable for the case studied since the rotating rolls of the machine impose defects on the final product which periodically repeat themselves. Moreover, the filter design changes according to the observed signal, being in this way signal adaptive. The properties listed above represent the main advantages of this method compared to the traditional filtering approach, such as comb filters or FFT filters [11].

Another property that makes these filters suitable for this application is that they are not limited in the frequency resolution by the sampling frequency. This means that the input fundamental frequency can be chosen as needed. Moreover, these filters have excellent performance even in presence of two closely spaced sources when dealing with a multi-pitch signal [8]. Nevertheless, there is a limit to the ability of the filter in separating two frequencies that are very close to each other. This is an important aspect to consider since in paper machines many rolls have similar diameters and therefore similar rotational frequencies. The difference between two rotational frequencies can reach even values lower than 0.01 Hz.

In addition to all the mentioned properties, the optimization procedure leads to filters that seek to suppress strong interfering sources [8], i.e. other periodic sources, which is crucial considering the number of machine components in paper production. Overall, the APES-based method proved to be efficient for different values of signal to noise ratio (SNR) and signal to interference ratio (SIR), presenting several advantages over the Capon-based one, which can be derived as a special case of it [11]. The Capon-based method offers the worst performance in terms of estimation of amplitudes and phases of the harmonic components since it is not optimized to have a periodic output and performs poorly for high SNRs because it suffers from bad conditioning of the covariance matrix. On the other hand, the major drawback of the optimal filtering approaches is the associated computational complexity [11].

2.3.1. Implementation of the method

In this section, the mathematical implementation of the filter is repeated and explained using references [8], [11], and [15].

Before starting, it is necessary to define the model of the signal. The signal is assumed to be periodic and each periodic component, termed a source, consists of a weighted sum of sinusoids with frequencies that are integer multiples of a fundamental frequency ω_k. Each source represents a component of the machine and, since more than one component generally affects the quality variation, a multi-pitch signal model should be used. Equation 2.1 shows the equation of the signal where noise, modeled as originated by a single source and supposed to be zero-mean, Gaussian, and white is added. Each source is indexed by k, while l denotes the harmonic component of the source and can have a maximum value of L_k which is the total number of sinusoids for each source. $A_{k,l}$ is the amplitude value of the lth harmonic of the source and $\phi_{k,l}$ is the phase of the harmonic, which is uniformly distributed on $(-\pi, \pi]$.

$$x(n) = \sum_{k=1}^{K} x_k(n) = \sum_{k=1}^{K} \sum_{l=1}^{L_k} A_{k,l} \sin(\omega_k l n + \phi_{k,l}) + e(n) \qquad n = 0, ..., N-1. \tag{2.1}$$

The filter operates on a vector containing M consecutive time-reversed samples of the observed signal

$$\mathbf{x}(n) = \begin{bmatrix} x(n) & x(n-1) & \dots & x(N-M+1) \end{bmatrix}^T, \tag{2.2}$$

that can be written in matrix form as in Equation 2.6, where $\mathbf{D}^n$ is defined in Equation 2.7. $\mathbf{Z}_k \in \mathbb{C}^{M \times 2L_k}$ is a Vandermonde matrix (Eq. 2.3), built from $2L_k$ harmonically related complex sinusoidal vectors (Eq. 2.4) and $\mathbf{a}_k$ is defined in Equation 2.5, where $a_{k,l} = \frac{A_{k,l}}{2} e^{j\phi_{k,l}}$, * represents the complex conjugate operator, and H is the Hermitian transpose operator.

$$\mathbf{Z}_k = \begin{bmatrix} \mathbf{z}(-\omega_k) & \mathbf{z}(\omega_k) & \dots & \mathbf{z}(-\omega_k L_k) & \mathbf{z}(\omega_k L_k) \end{bmatrix}. \tag{2.3}$$

$$\mathbf{z}(\omega) = \begin{bmatrix} 1 & e^{-j\omega} & \dots & e^{-j\omega(M-1)} \end{bmatrix}^T. \tag{2.4}$$

$$\mathbf{a}_k = \begin{bmatrix} a^*_{k,1} & a_{k,1} & \dots & a^*_{k,L_k} & a_{k,L_k} \end{bmatrix}^H . \tag{2.5}$$

$$\mathbf{x}(n) = \sum_{k=1}^{K} \mathbf{Z}_k \mathbf{D}^n \mathbf{a}_k^* + \mathbf{e}(n) \triangleq \sum_{k=1}^{K} \mathbf{Z}_k \mathbf{a}_k^*(n) + \mathbf{e}(n) \triangleq \sum_{k=1}^{K} \mathbf{Z}_k(n) \mathbf{a}_k^* + \mathbf{e}(n) \tag{2.6}$$

$$\mathbf{D}^n = \begin{bmatrix} e^{-j\omega_k 1 n} & & & & \\ & e^{j\omega_k 1 n} & & & \\ & & \ddots & & \\ & & & e^{-j\omega_k L_k n} & \\ & & & & e^{j\omega_k L_k n} \end{bmatrix} \tag{2.7}$$

When the filter, defined by the vector of coefficients

$$\mathbf{h}_k = \begin{bmatrix} h_k(0) & \dots & h_k(M-1) \end{bmatrix}^H , \tag{2.8}$$

is applied to the vector of M time-reversed samples of the observed signal, i.e. $\mathbf{x}(n)$, the output $y_k(n)$ is produced (Eq. 2.9).

$$y_k(n) = \sum_{m=0}^{M-1} h_k(m) x(n-m) \tag{2.9}$$

The expected output power of the filter is

$$E\{|y_k(n)|^2\} = E\{\mathbf{h}_k^H \mathbf{x}(n) \mathbf{x}^H(n) \mathbf{h}_k\} = \mathbf{h}_k^H \mathbf{R} \mathbf{h}_k, \tag{2.10}$$

where

$$\mathbf{R} = E\{\mathbf{x}(n) \mathbf{x}^H(n)\}. \tag{2.11}$$

is the covariance matrix of the observed signal which, with the hypothesis of statistically independent sources, can be written as

$$\mathbf{R} = \sum_{k=1}^{K} \mathbf{R}_k = \sum_{k=1}^{K} E\{\mathbf{x}_k(n)\mathbf{x}_k^H(n)\}. \tag{2.12}$$

Substituting in the last equation the model of the signal in Equation 2.6, it is possible to rewrite the covariance matrix as

$$\mathbf{R} = \sum_{k=1}^{k} \mathbf{Z}_K E\{\mathbf{a}_k^*(n)\mathbf{a}_k^T(n)\}\mathbf{Z}_k^H + E\{\mathbf{e}_k(n)\mathbf{e}_k^H(n)\} = \sum_{k=1}^{K} \mathbf{Z}_k \mathbf{P}_k \mathbf{Z}_k^H + \mathbf{Q}, \tag{2.13}$$

where matrix $\mathbf{P}_k$ is the covariance matrix of the complex amplitudes of the harmonics, expressed as time-varying quantities, and $\mathbf{Q}$ is the noise covariance matrix (Eq. 2.14).

$$\mathbf{Q} = E\{\mathbf{e}(n)\mathbf{e}^H(n)\} = \sum_{k=1}^{K} \mathbf{Q}_k. \tag{2.14}$$

Since the covariance matrix is unknown in practical situations, it is replaced with an estimation (Eq. 2.15).

$$\hat{\mathbf{R}} = 1/G \sum_{n=M-1}^{N-1} \mathbf{x}(n)\mathbf{x}^H(n) \qquad \text{where} \quad G = N - M + 1. \tag{2.15}$$

To obtain an invertible covariance matrix, it is necessary to have $M < N/2+1$. The filter coefficients, $\{h_k(m)\}$, are selected as the coefficients which minimize the mean square error (MSE) between the filter output and the desired output.

The desired output is a harmonic signal which can be defined as

$$\hat{y}_k(n) = \sum_{l=1}^{L_k} a_{k,l} e^{j\omega_k l n} = \mathbf{a}_k^H \mathbf{w}_k(n). \tag{2.16}$$

The function to be minimized can be therefore written in the following form:

$$P = \frac{1}{G}\sum_{n=M-1}^{N-1} |y_k(n) - \hat{y}_k(n)|^2 = \frac{1}{G}\sum_{n=M-1}^{N-1} |\mathbf{h}_k^H \mathbf{x}(n) - \mathbf{a}_k^H \mathbf{w}_k(n)|^2. \tag{2.17}$$

Defining the new quantities

$$\begin{aligned} \mathbf{G}_k &= \frac{1}{G}\sum_{n=M-1}^{N-1} \mathbf{w}_k(n)\mathbf{x}^H(n) \\ \mathbf{W}_k &= \frac{1}{G}\sum_{n=M-1}^{N-1} \mathbf{w}_k(n)\mathbf{w}_k^H(n), \end{aligned} \tag{2.18}$$

Equation 2.17 can be rewritten as

$$P = \mathbf{h}_k^H \hat{\mathbf{R}} \mathbf{h}_k - \mathbf{a}_k^H \mathbf{G}_k \mathbf{h}_k - \mathbf{h}_k^H \mathbf{G}_k^H \mathbf{a}_k + \mathbf{a}_k^H \mathbf{W}_k \mathbf{a}_k. \tag{2.19}$$

Minimizing the previous equation with respect to the complex amplitudes, the result obtained is

$$\hat{\mathbf{a}}_k = \mathbf{W}_k^{-1} \mathbf{G}_k \mathbf{h}_k. \tag{2.20}$$

With some manipulation, Equation 2.19 can be simplified as

$$P = \mathbf{h}_k^H \hat{\mathbf{Q}}_k \mathbf{h}_k \qquad \text{where} \quad \hat{\mathbf{Q}}_k = \hat{\mathbf{R}}_k - \mathbf{G}_k^H \mathbf{W}_k^{-1} \mathbf{G}_k. \tag{2.21}$$

$\hat{\mathbf{Q}}_k$ is the modified covariance matrix, which is obtained by subtracting from the estimated covariance matrix the contribution of the harmonics the filter has to extract. It should be noted that in this derivation both the fundamental frequency and the number of harmonics are supposed to be known. The set of filter coefficients is the one that minimizes the last expression of P, obtained in Equation 2.21.

To obtain a non-trivial solution, additional constraints must be added to the problem. These additional constraints force the filter to have unit gain, at all the harmonic frequencies to be extracted. In this way, the obtained filter passes undistorted the content at the extracted frequencies.

The filter design problem can be thus written as

$$\min_{\mathbf{h}_k} \mathbf{h}_k^H \hat{\mathbf{Q}}_k \mathbf{h}_k \quad s.t. \quad \mathbf{h}_k \mathbf{z}(\omega_k l) = 1, \quad \text{for} \quad l = 1, \ldots, L_k. \tag{2.22}$$

The problem of finding the filter coefficients, expressed in Equation 2.22, is, therefore, a convex optimization problem with equality constraints, which can be solved with the Lagrange multiplier method. After some computations the result obtained is

$$\hat{\mathbf{h}}_k = \hat{\mathbf{Q}}_k^{-1} \mathbf{Z}_k (\mathbf{Z}_k^H \hat{\mathbf{Q}}_k^{-1} \mathbf{Z}_k)^{-1} \mathbf{1}. \tag{2.23}$$

2.3.2. Hypothesis and parameters

Before proceeding with the implementation, it is important to be aware of some hypotheses the filter is based on and the criteria to follow in the choice of the filter parameters.

One of the hypotheses made in the theoretical derivation of the filter design is that the signal is stationary over the entire length N, which represents the duration of the observation [11]. The length of the signal and, consequently, also the filter length M, are limited by this constraint. Moreover, as already mentioned, the value M must be lower than $N/2 + 1$ to ensure that matrix $\hat{\mathbf{R}}$ is invertible and, additionally, the accuracy of the matrix $\hat{\mathbf{R}}$ increases when M decreases. On the other hand, the higher the filter length, the better the performance of the filter in attenuating noise and canceling interference sources [11]. The reason is that the filter used in this thesis is a bandpass filter with an impulse response aperture equal to M and a resolution of $1/M$ [16]. Therefore, the higher M is, the better the resolution and the more accurate the result. The filter length should be chosen considering all these factors and the additional limitation given by the computational complexity, which increases with M.

Another assumption of the method is that the signal to be extracted is composed of a limited number of harmonics, called model order, which is assumed to be known. In practice, a signal is composed of an infinite number of harmonics. The optimization procedure is therefore just an approximation when dealing with real signals. The number of harmonics has to be chosen according to the application. The target is to reproduce the most significant part of the signal, considering that the higher the model order the more interfering sources the filter can deal with, at the expense of the computational complexity [11]. The model order can also be estimated using a method, called MAP rule [17], which seeks to find the number of harmonics that maximizes the a posteriori probability of the model order given the observation. Another approach is to use the hMUSIC algorithm which can jointly estimate the model order and the fundamental frequency, another required input of the filter. The hMUSIC algorithm is a subspace method based on finding the values of model order and fundamental frequency for which the signal subspace, represented by the Vandermonde matrix, is closest to being orthogonal to the noise subspace [12].

Another assumption of the APES filter is to have white and Gaussian noise. The Gaussian assumption appears to be the norm in literature and, even when the assumption does not hold, the method can still be considered accurate, at least asymptotically [18]. The white Gaussian distribution, instead, can be shown to be the one that maximizes the entropy of the noise, representing the worst-case scenario [18]. In case the problem involves a non-white noise, a pre-whitener, i.e. a filter that makes the stochastic part of the signal white, can be applied. This method extracts a pre-whitening matrix that reduces the noise covariance matrix to an identity matrix when the two are multiplied. This procedure works well when the noise is stationary and when measurements where only the noise is present are available [8]. In the frequency domain, the pre-whitener can be seen as a filter with a frequency response similar to the inverse of the spectrum of the noise [21]. If the signal is multiplied by the frequency response of the obtained filter, a flat spectrum for the noise is obtained. Naturally, the desired signal will also be altered by the passage through the filter, and this can affect the result, according to how much the signal is changed. To obtain the desired filter, information about the noise spectrum is needed [21]. Different methods exist to estimate the power spectral density (PSD) of the noise from a mixture of desired signal and noise. One possibility is to use a minimum mean-square error (MMSE) optimal estimation, obtained by the computation of the conditional expectation of the square of the noise given the observed signal [19]. Once the pre-whitener has been applied, it is possible to quantify the whiteness of the noise through the spectral flatness measure (SFM) parameter [20]. This parameter is defined as the ratio between the geometric and the arithmetic mean of the noise PSD. It can assume values between 0, in presence of more colored noise, and 1, which represents the case of perfect white noise.

The choice of the parameters and the compliance with the assumptions for this MD analysis application are discussed in the following chapter.

2.4. Sources of quality variation

Quality variation can be caused by changes in the raw material or problems related to the production process. The latter can be divided into three classes of malfunctions [23]. The first class, slow performance degradation, might be caused by the wearing or fouling of the equipment. The second class is represented by periodic fluctuations, caused by rotating equipment or, in the case of low-frequency variation, by upstream disturbances. The third class consists of sporadic phenomena caused, for example, by a violation of parameter limits. In this work, the focus is on periodic fluctuations caused by rotating equipment, particularly rolls.

In a previous thesis work [5], the author demonstrated, through the application of the hMUSIC algorithm, that in the signal coming from sensors positioned on the machine, it is possible to detect the presence of harmonic components with a fundamental frequency equal to the rotational frequency of some rolls in the machine. However, this discovery was not completely new. For example, in the 1990s, analyses made with the Tapio analyzer on lightweight coated (LWC) paper showed that the quality variation of thickness, basis weight, and ash in the machine direction presented a periodicity of two and three times the revolution of the backing roll [24]. In general, these periodic patterns are due to defects in the roll shape, caused by the manufacturing process, imperfections in the bearings, and errors in the mounting procedure.

To raise the production capacity, the running speed of the machines has been increased in the last decades, making vibration problems more significant. Vibrations affect the final quality of the paper, being even more dangerous when the frequency of vibration matches the natural frequency of a roll or, of the entire system.

The need to reduce vibrations forced roll manufacturers to find new and more precise production methods [28]. The first improvement in the roll machining technology consisted of compensating the slideway error of the machine tool, which causes systematic diameter variation to the roll in the axial direction. Successively, the trend in the roll manufacturing process moved towards the production of ideal geometry. The roundness error, which is due to the change in the distance between the workpiece center axis and the tool, was minimized as much as possible. Finally, the third generation of roll machining technology was introduced. This technology takes into consideration that the geometry of the roll changes between the roll machining shop environment and the production environment. This change is related to factors such as speed, temperature, and load that can cause roll deflection and deformation. To compensate for all these effects, the roll geometry is optimized according to the production environment [28]. Despite the effort in improving the roll manufacturing process, it is not possible to eliminate all the sources of quality variation.

2.4.1. Roll model

A rotor is called rigid or flexible depending on the characteristics of the rotor itself but also of bearings and foundation [31]. According to the definition present in the ISO standard 21940-12 (2016), a rotor can be considered rigid for balancing purposes if the first flexural resonance speed exceeds the maximum service speed by at least 50%.

Generally, rolls in paper machines are flexible rotors [28]. This means that their behavior changes as a function of the rotational speed, due to the change in the state of balance. Rolls can be modeled as homogeneous, flexible beams with an indefinite number of eigenmodes and natural frequencies [31]. When the rotational frequency equals the natural frequency of one mode, huge vibrations occur, even in presence of a small excitation force.

Usually, the natural frequency of flexible rotors is identified as the natural frequency of the first bending mode [24]. It is also possible to experience a resonant behavior when the angular velocity is an integer fraction of the natural frequency, i.e. subharmonic resonances. For example, when the rotational frequency halves the natural frequency, the roll still vibrates at the natural frequency, due to errors such as bending stiffness variation or ovality of the roll geometry, both effects that cause excitation twice per revolution. Large flexible rotors are usually operated at a speed lower than the critical speed, i.e. the natural frequency of the first bending mode, or lower than the half-critical speed [24].

Figure 2.3 shows some of the eigenmodes of a roll. The dashed line represents the static ideal configuration of the roll. The nodes of the eigenmodes are the sections of the roll that remain always in the position they assume in the static configuration. At these points, the amplitude of the vibration is null; therefore, the quality variation is not affected.

2.4.2. Roll run-out

The term run-out can be used as a general term to identify deviations from the ideal shape and behavior of a roll. Run-out is defined by the standard ISO 1101 (2017) as a radial variation from a true circle. The most common way to express it is using a peak-to-peak value, i.e. the difference between the maximum and the minimum value, of the sum of all the error components [24]. The latter is evaluated considering the rotor central axis

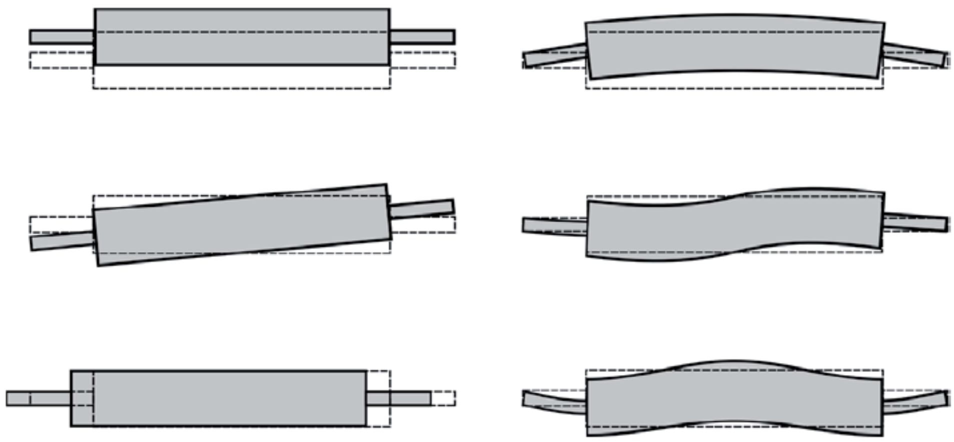

Figure 2.3: Some eigenmodes of a roll; translational rigid body modes (left) and bending modes of a flexible rotor (right). The dashed line represents the static ideal configuration of the roll. [24].

movement and the rotor surface roundness profile [32].

Run-out can be classified into static and dynamic [24]. The first one can be caused, for example, by initial bending (not gravitational), roundness error, and bearing error motion. The second one includes the components that change as a function of the rotating frequency, and it is caused by bending due to unbalance, deformation of the roll shell, bending stiffness variation, or excitation from the paper or other parts of the machine, for instance [24].

Unbalance is one of the most prominent faults occurring in rotors and one of the most common sources of vibration. It derives from manufacturing inaccuracies, limited tolerance in parts, inhomogeneous material, and imprecise assembly [29]. It can be minimized by a balancing procedure, but balancing classes allow a certain amount of residual unbalance. This can become more significant after a certain period of operation, due to wear and accumulation of dirt. Therefore, it is necessary to monitor vibrations and perform diagnostics. Moreover, flexible rotors can be optimally dynamically balanced only at a certain rotating frequency [29]. Unbalance can be defined as a combination of two ideal unbalanced states [24]. The first is the static unbalance, according to which the rotational axis and the central principal axis are parallel but not coincident. The second one is the dynamic unbalance, caused by the fact that the two axes are not parallel. The unbalance causes deflection of the roll, vibrations, and rotating force on bearing supports, producing variations of paper parameters in the machine direction with a harmonic frequency equal to the rotational frequency of the roll affected by the unbalance. It represents one of the main causes of roll dynamic deflection together with thermal bending, which is caused by inhomogeneous material structure and uneven thermal distribution, and tension of the paper web or felt [24].

Bending stiffness variation (BSV), instead, is caused by the asymmetry in the principal axes of inertia in the cross-section of the roll, and it is caused by rotor geometry errors, material inhomogeneity, and structural discontinuities [24]. BSV excitation is enabled when the rotor is bent under the effect of gravity, by loads in the process, or by other excitations [30]. The center point of the roll whirls at a speed that doubles the rotational speed of the rotor, causing variations in the final product with a frequency equal to 2ω, where ω is the rotational frequency of the roll [24]. The problem of vibration is especially dangerous when the rotational speed equals half the critical speed. Most BSV is caused by geometrical errors, such as shell thickness variation, grooves in the shell, welded seams, keyways, or other manufacturing errors [30]. In [30], the author demonstrated that, typically, BSV is mainly induced by the lowest roundness components, especially by the second one. Additionally, the magnitude of BSV is dependent on the amplitude of the components and the profile location since moments are larger in the middle of the rotor.

Vibration is also caused by the geometrical errors of the bearing components, such as thickness variation of the inner and outer rings, roundness errors, and diameter variation of balls or rollers. Most of the excitation induced by bearings is not synchronized with the rotation of the rotors, except for the excitation caused by the rotating ring, which is synchronized with the roll speed [31]. The roundness profile of a bearing inner ring, in the case in which the outer ring is fixed and the inner ring is rotating, is composed of the rotor shaft roundness profile at the bearing installation cross-section, the thickness variation of the bearing inner ring, and the adapter sleeve if present [33]. The inner ring and the adapter sleeve are flexible, compared to the shaft, thus adapting to the roundness profile of the shaft [31]. The excitation frequency of bearing elements is a multiple of the rotational frequency of the shaft and the number of undulations of the roundness profile of the inner ring [33]. The amplitude of excitation depends on the phase angles of the waviness components of the roundness profiles of the two bearings, being lower if the phase angles differ from each other [31].

A resonance vibration is induced when the rotational frequency is a submultiple of the natural frequency. This excitation is transmitted to the roll together with vibrations coming from other parts of the machine, generally called frame vibrations. Frame vibrations can be transmitted not only by the bearings but also by the driving shaft, or any other component which is in contact with the machine [24]. Other sources of vibrations include felts, wires, pumps, and tension variations of the paper web. The excitation can be reduced by improving the dynamic behavior of the roll, i.e. the manufacturing accuracy.

In the roll manufacturing process, various conditions can result in some deviation from the ideal shape, such as roundness error, axial diameter variation, cylindricity, conicity of the shell, straightness, thickness of the shell, unbalance, and surface roughness. One of the most significant causes of roll manufacturing inaccuracy is the guideway error. It consists of a non-perfect straight tool motion, which is copied into the geometry of the roll, affecting the straightness and the axial diameter variation [28]. Another cause of axial diameter variation is the non-perfect alignment between the rotational axis of the roll and the tool path, which leads to a conical geometry after machining [24]. In the machining process, the workpiece also presents an error in the rotational motion, which gives rise to a changing distance between the roll center axis and the tool. The main reasons for this rotational error are the change in flexural stiffness and the accuracy of the bearing arrangement [28]. In the case of the bearing arrangement, the cause is the roundness error of the rotating inner ring, determined by the roundness error of the shaft, the variation in thickness of the conical adapter sleeve, and the variation in thickness of the inner ring. The result is a non-round profile of the roll after machining.

For example, Juhanko and Väänänen [27] demonstrated in 1999 that the adapter sleeve was a possible cause of the ovality of the roll. Even the bending stiffness variation causes a final oval geometry since the center axis is moving with a frequency two times higher than the rotational speed. The amount of ovality is also affected by the bending due to the gravity force.

An additional problem that can be encountered during machining is the presence of a gradual one-sided temperature distribution in the workpiece. This uneven thermal distribution can cause bending of high scale, considering that the thermal expansion coefficient of steel is 10 μm °Cm^{-1}, but the problem can be minimized by rotating the roll before machining [24].

2.4.3. Roundness error

Roundness can be defined as the minimum radial distance between two concentric circles, with equal center points, inside and outside the roundness profile (Figure 2.4). According to the ISO 12181-1 and 2 standards, a roundness profile can be divided into harmonic components and, therefore, be represented by a Fourier series. Figure 2.4 represents one example of a roundness profile with the corresponding first 30 amplitude terms of its Fourier series. For example, the first harmonic represents an eccentric movement, the second corresponds to ovality, the third to triangularity, and the fourth to squareness.

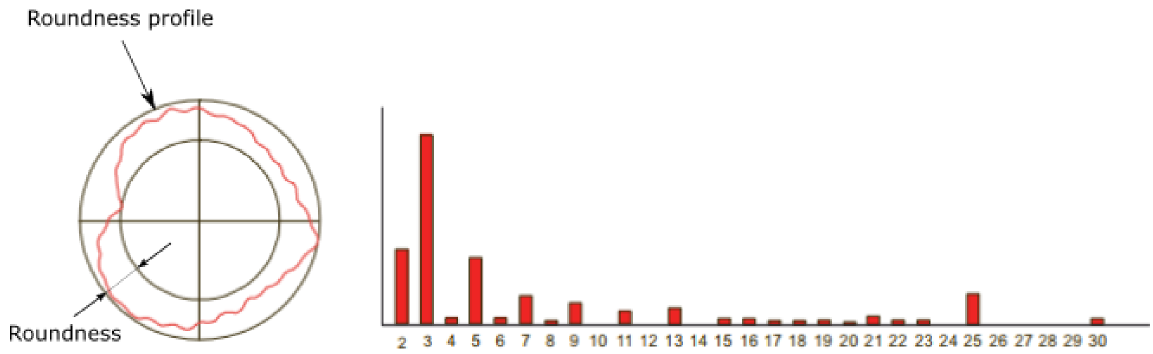

Figure 2.4: Roundness profile and definition of roundness (left); amplitude terms of the Fourier series of the roundness profile (right) [24].

Usually, a rotor contains only one or a small number of dominant components [30].

To measure roundness, it is necessary to separate the effect of the rotating center point motion and the roundness profile from the run-out signal. Since rolls are too large to be placed onto a high precision spindle, alternative ways based on multi-probe measurement have been developed [25]. This type of method is needed for large flexible rotors, because the center point motion is unpredictable and unrepeatable, due to factors such as the presence of random loads and bending stiffness variation contributing to the error motion. Despite the arbitrariness, a decreasing trend of center point harmonic component amplitudes has been measured in a large flexible rotor [33]. This assumption has been used in [25] to compare three different multi-probe measurement methods: a three-point method, a least-squares four-point method, and a redundant diameter four-point method. In particular, the three-point method yielded the smallest total error distributions for the harmonic components and the most accurate and least uncertain estimate for total roundness. The roundness profile of a roll cross-section changes with the rotational speed [24]; therefore, this is an additional element to consider when measuring the roundness.

Roundness errors can be induced by vibrations of the roll synchronous with the rotation, occurring during the machining process [28]. The roundness of the rolls needs to be maintained at the highest possible level, as it can induce localized and system-wide vibration, directly impacting the quality of the end product [26].

When two rolls affected by roundness error are in contact and pressed together forming a nip, a phenomenon called barring can occur [24]. Barring is a vibration mechanism due to the growth of corrugation of certain wavelengths from roll irregularities [28]. It usually happens in the paper machine calenders and the press section.

3 | Materials and methods

3.1. Available data

Basis weight, moisture, and caliper data are available to develop the work. These data have been acquired with measurements performed offline and online, on the same strip of cardboard, 1.1 km long. Online measurements are acquired with a quality control system (QCS), which is placed on a paperboard machine operating at a speed of 600 $\frac{\mathrm{m}}{\mathrm{min}}$. The system consists of a measurement platform that moves across the web guided by a scanner beam (Figure 3.1). To detect only MD variations, the probe is held stationary in correspondence to a point sufficiently distant from the edges.

The following is a brief description of the sensors referring to [3] and [34]. The basis weight estimation is based on the amount of beta radiation, provided by an enriched Kr85 nuclear source, absorbed by the mass of paper or board sheet. The transmitted radiation is captured and measured by an ion chamber type detector. Moisture is estimated based on the quantity of radiation absorbed by the water in the product. Microwave and infrared radiation are used and, in both cases, the property of water to absorb only certain wavelengths of the beam is exploited. The caliper sensor, instead, is composed of a magnetic coil in the upper measurement head and a ferrite plate in the lower one. The magnetic coil is connected to an oscillator that transforms the current generated by the changes in the distance between the coil and the ferrite plate into voltage pulses. When a contact sensor is used the upper and the lower head are in contact with the sheet. In non-contact measurements, the magnetic principle is used to measure the distance of a laser to the reference plate, while the non-contacting laser triangulation optical principle measures the distance to the paper surface.

The sampling frequency of the data from the QCS is 25 Hz and this causes a limitation in the maximum frequency that can be detected. According to the Nyquist theorem $f_{max} = \frac{f_s}{2}$. Since the velocity of the machine is 600 $\frac{\mathrm{m}}{\mathrm{min}}$, the distance between two measured points is 0.4 m.

Offline measurements are obtained with a system developed by Tapio Technologies com-

Figure 3.1: QCS placed at the end of the paper machine to perform online measurements. The system consists of a measurement platform that moves across the web guided by a scanner beam (picture downloaded from [34])

pany (Figure 3.2). This system allows having higher resolution data, 40 times higher than the one of online measurements. Moreover, the software can perform different types of analysis, including one able to separate the original signal (SOS) from the noisy mixture.

Additionally, the diameter of each roll in the machine is known. The rotational frequency of the rolls is computed as the ratio between the machine speed and the roll diameter. The values of diameter and frequency of the rolls are reported in Appendix A.1.

Figure 3.2: Tapio analyzer (picture downloaded from [35])

3.2. Matlab implementation

This section provides a brief explanation of the step to follow in the filter application. A Matlab implementation of the filter is used. The filter requires as input the real signal, the fundamental frequency ω_0, normalized according to Equation 3.1, the model order, and the filter length. The filter length M is selected equal to the length of the signal divided by 4, in agreement with what was said in the literature review. The function returns as output the set of filter coefficients to apply to the signal to obtain the desired one.

$$\omega_{norm} = \frac{2\pi\omega_0}{f_s} \tag{3.1}$$

The filter always produces a transient of length M on the output signal. The amplitude values of the extracted signal are estimated by applying a harmonic model fitting, after removing the transient. The harmonic model fitting finds the complex amplitudes vector to best fit a real signal through a least square estimation, reported in Equation 3.2, where $\mathbf{Z}$ is the Vandermonde matrix already defined in 2.3, and $\mathbf{x}$ is the signal.

$$\mathbf{a} = (\mathbf{Z}^H\mathbf{Z})^{-1}\mathbf{Z}^H\mathbf{x} \tag{3.2}$$

3.3. Synthetic signal for preliminary testing

The method is first applied to a synthetic signal. This procedure is carried out to evaluate the possible limitations of this filter in the industrial field. Indeed, in the real application, the hypotheses of the method are not entirely satisfied. The following chapters investigate the possible deviations from the ideal condition, in which all the hypotheses of the filter are satisfied, and the related errors. The generated signal is a mixture of periodic components and noise, built to reproduce as faithfully as possible the behavior of the real signal acquired by the sensors. Specifically, the signal is built referring to the caliper measurements, acquired by the Tapio analyzer. Data from the Tapio analyzer are preferred over the QCS data because of the higher sampling frequency and the lower level of noise.

3.3.1. Behaviour of the amplitude values of the harmonic components

To derive a general trend of the amplitude values of the harmonic components, the filter is applied to the caliper signal measured with the Tapio analyzer. The effect of 5 different rolls is extracted, applying the filter with different input base frequencies. The 5 fundamental frequencies are selected from the rolls list available. Since the signal is quite long, it is split into five segments of equal length, and the filter is applied to each segment, for each fundamental frequency. The estimated amplitude values of the harmonic signal for a given fundamental frequency are computed as the average of the results obtained for the different segments.

The bar plots in Figure 3.3 show the amplitude values for the selected fundamental frequencies. The Tapio data are low pass filtered and the highest frequency detectable in the signal is around 200 Hz. This explains why the bar plots for the two higher fundamental frequencies have a zero-amplitude value for high harmonic numbers. In all the cases there is a decreasing trend of the harmonic amplitudes increasing the harmonic number, and the first harmonic component has always the highest value. The amplitude values are interpolated with a decreasing exponential function of the form ae^{-b}. For the two harmonic series with the highest amplitude value of the first harmonic component, the parameter b is higher, being the decreasing trend steeper.

According to these considerations, a function to generate the amplitude values is implemented. In this function, the value for the first harmonic component is generated as a random value between 0.12 and 1.5. This value corresponds to the parameter a of the exponential function. The parameter b of the exponential is randomly generated in a way that it is higher for higher values of the first harmonic component amplitude. The amplitude values for all the other harmonic components are generated using the exponential function with parameters a and b. To better reproduce the actual behavior, random values are added or subtracted, from each component. Figure 3.4 reports two examples of the generated amplitudes. Once the amplitude values are obtained, phase values are randomly generated between $(-\pi, \pi]$, and a sum of sinusoidal functions is built according to the base frequency.

The final generated signal is composed of the sum of 9 harmonic series. The base frequencies of the series are chosen from the list of rotational frequencies of the rolls in the machine. The choice of selecting just 9 rolls, and not all of them, is due to computational reasons. However, even if in a paper machine more rolls are present it is reasonable to think that not all the rolls have an impact on the quality variation simultaneously.

3.3.2. Real noise analysis

According to the hypothesis of the filter, the noise is supposed to be white and Gaussian. As shortly discussed in the literature review, noise trackers can be used to estimate the PSD of the noise and a pre-whitener can be applied to transform the stochastic part of the signal. However, this procedure is applicable only if a portion of the signal where the only noise is present is available. In the case of paper production, it is not possible to obtain this data since the noise is present only when the machine is running. It is therefore impossible to separate the desired signal from the noise.

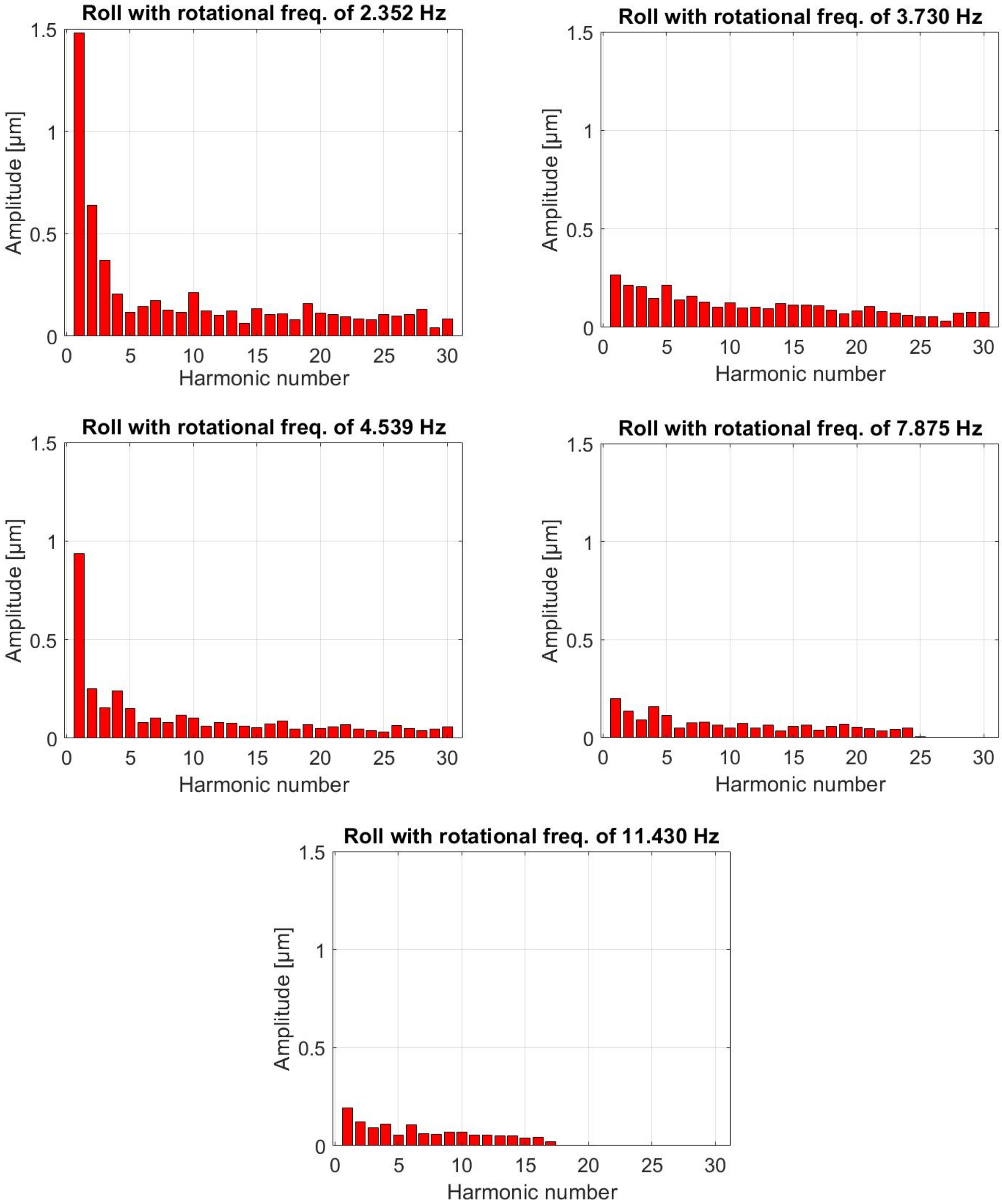

Figure 3.3: Amplitude values of the harmonic components obtained by applying the filter to the caliper signal. The effect of five different rolls is reported.

The noise in the paper machine environment comes from the vibration of the machine itself and electrical components. The signals coming from the QCS and Tapio analyzer are studied and compared to extract information about the noise. The PSDs of the two signals in Figure 3.5 have two peaks at frequencies close to 2.3 Hz and 4.5 Hz. These two

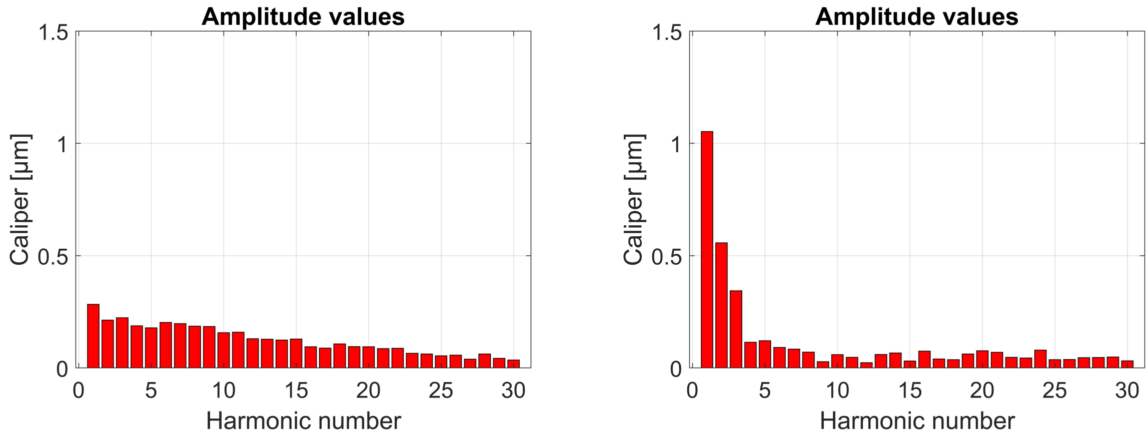

Figure 3.4: Examples of generated harmonic series.

peaks correspond to the rotational frequencies of two rolls in the machine, and they are, therefore, for sure part of the deterministic signal. These two frequencies are removed from the signal with two band-stop filters. The PSDs are then computed again, and their RMS is computed at intervals of 2 Hz. Figure 3.6 shows the final plot of the RMS values. Even if the PSDs still contain deterministic components and, therefore, do not represent the only noise, some observations can be done. In both cases, the energy content of the signals decreases increasing the frequency value. Additionally, especially in the set of data acquired on the machine the energy content at low frequencies is quite high.

The PSD is far to be flat, as it should be in presence of white noise. Therefore, the noise cannot be considered white. The high energy content at low frequencies makes the noise more similar to a pink noise. The same decreasing trend of the energy content is observed in the basis weight data. The Gaussian assumption, instead, can be considered more realistic. Figure 3.7 shows that the probability distribution of the data does not depart much from a Gaussian distribution, represented by the red line.

3.3.3. Studied cases

This chapter presents the different studied cases analyzed to reproduce conditions that depart from the hypotheses of the filter or can represent critical situations. The aim is to understand how the filter behaves in these cases to verify if it is possible to obtain a satisfying result and propose possible solutions to improve the performance.

As already mentioned, the noise present in the machine environment is reasonably not white. To understand how the filter behaves with a different type of noise, the presence of pink noise is also analyzed. Moreover, different noise amplitudes are tested to understand

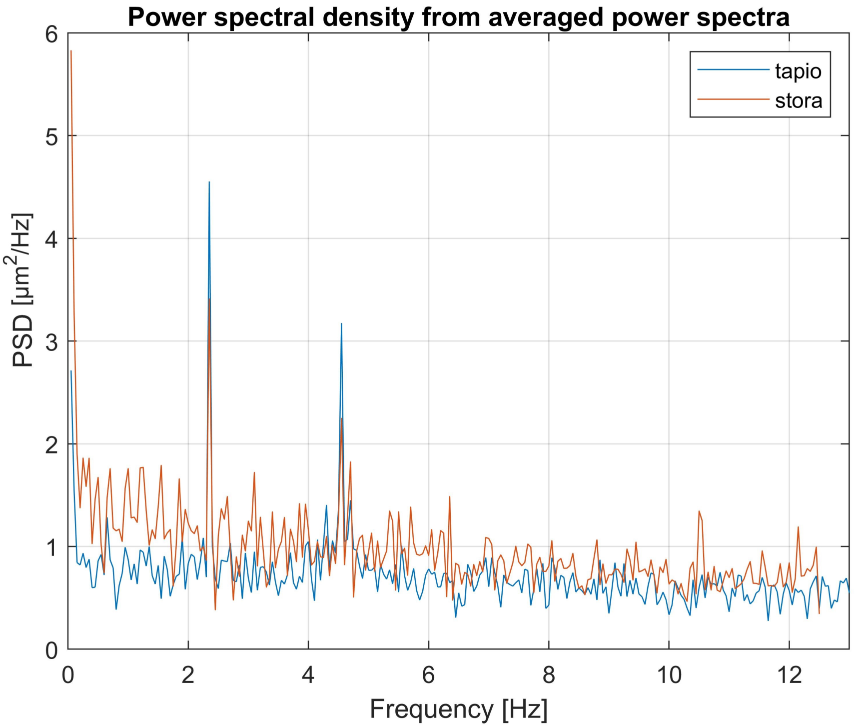

Figure 3.5: PSDs of the spectra computed from the average of PS for QCS (stora) and Tapio data.

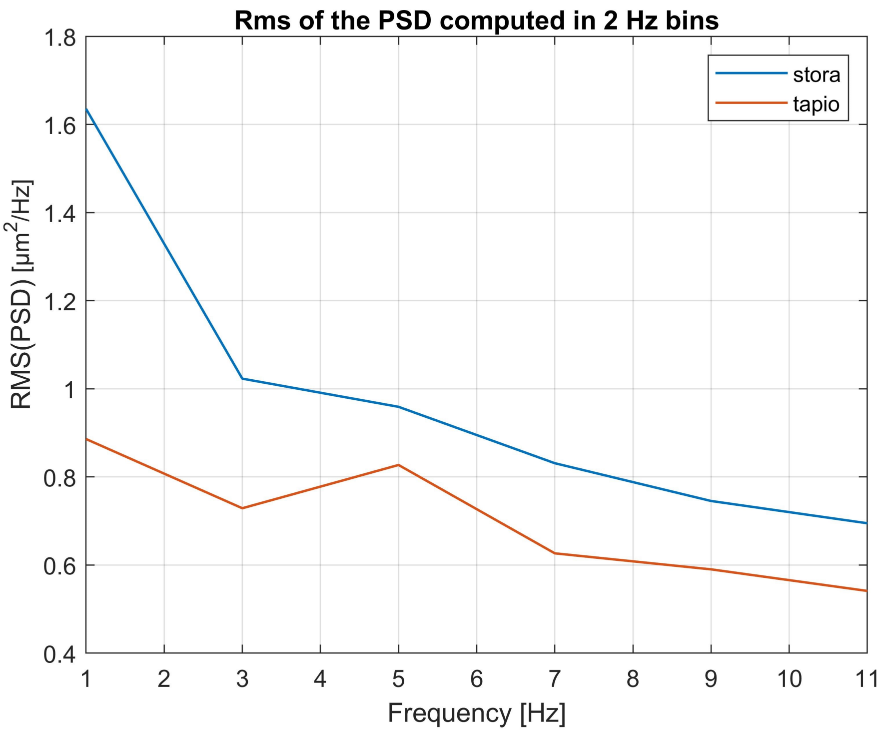

Figure 3.6: RMS of the PSDs of QCS (stora) and Tapio data computed for bins of 2 Hz.

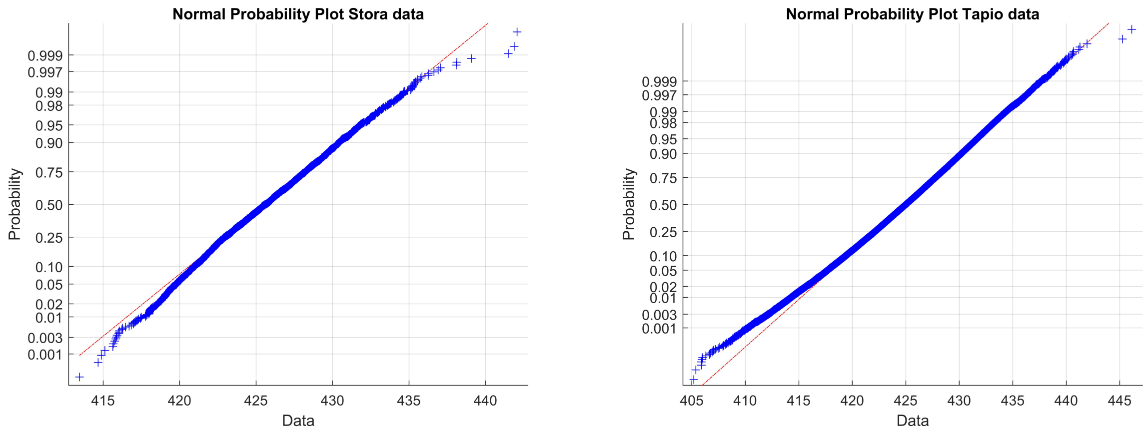

Figure 3.7: Normal probability plots of QCS (stora) data (left) and Tapio data (right).

the level of noise the method can deal with. An additional test is done considering a sudden variation of the noise amplitude during the acquisition time, to reproduce possible non-stationarity in the signal.

Additionally, the filter requires as input a fundamental frequency to extract. This frequency is chosen from the list of known roll rotational frequencies. However, in some situations, the frequency of variation of the quality parameter does not exactly correspond to the set point of the roll speed or to a multiple of that. The two frequencies are perfectly related only if the actual rotational frequency of the roll is exactly equal to the set point, and the frequency of variation remains the same from when the defect is generated until when it is measured.

The second condition is verified when the hypothesis of constant volume is valid. When the volume remains constant a decrease in the cross-sectional area leads to an increase in the product velocity (Equation 3.3). When the product passes through the rolls the material stretches and the distance between defects increases (Figure 3.8). However, the thickness of the paper decreases as well, and therefore, under the hypothesis of constant volume, the velocity increases. Consequently, the frequency of occurrence of defects remains constant. However, the hypothesis of constant volume is an approximation. It can happen that the speed does not increase in the same proportion as the thinning causing a slight mismatch between the rotational frequency and the frequency of quality variation. Moreover, the roll rotational frequency is not always exactly equal to the set point. Indeed, a common control strategy adopted during the production process consists in adjusting the rotational frequency making it oscillates around the set point.

$$A_0 v_0 = A_1 v_1 \tag{3.3}$$

This situation is reproduced by giving a wrong input frequency to the filter, i.e. a frequency slightly different from the one present in the signal. Naturally, when the input frequency is not coincident with the frequency present in the signal the performance decreases. A possible solution is proposed to reduce the error introduced by this mismatching. It consists in performing a frequency detection before extracting the result. Firstly, a range of frequencies containing the set point of the rotational frequency of the roll is defined. Subsequently, the filter is applied for the frequencies of the interval chosen, starting from the lowest one, and, finally, the non-captured power is computed. The algorithm stops when a minimum of the non-captured power, i.e. the maximum of the output power, is found. The frequency corresponding to the minimum is selected and used to extract the final result.

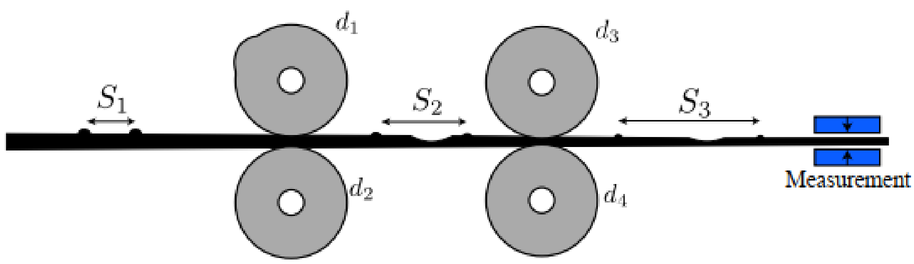

Figure 3.8: Distance between defects along the machine. When the product passes through the rolls the material stretches and the distance between defects increases.

The case of two close frequencies is also studied to understand when the filter can separate the effect of two sources with similar frequencies. This is important because in paper production many rolls have similar frequencies (cf. Appendix A.1). Another test was done by applying the filter to a non-stationary signal, in particular a chirp signal, i.e. a signal where the frequency linearly increases in time. Finally, the extraction of a frequency that is not present in the signal or a harmonic series where one harmonic is missing is simulated considering different SNRs.

Firstly, performance and computational time are evaluated with different window lengths. A compromise between the two is found, and the selected window length is used to perform all the tests.

3.3.4. Performance evaluation

The results are evaluated by computing the signal to distortion ratio (SDR). The parameter is calculated as in Equation 3.4 where y is the extracted signal while $\hat{y}$ is the harmonic series of the generated signal the filter aims to extract. This parameter evaluates the similarity between the two signals. The closest the signals are, the lower the RMS value of their difference and the higher the SDR.

$$SDR = \frac{1}{rms(\hat{y} - y)} \tag{3.4}$$

Additionally, a comparison between the amplitude values of the different harmonic components of generated and extracted signals can be performed. A more qualitative approach is to plot the two signals in time overlapped. This approach can be useful to have a visual and fast understanding of the result.

4 | Results

This chapter shows all the obtained results. The first section reports the results obtained by applying the filter to the synthetic signal, while the second presents the outcome of the filter application on data measured on a strip of paperboard. Finally, the third section shows a comparison between the optimal filter and the SOS tool of the Tapio software, which is able, given offline data, to separate a periodic signal of interest from the noisy mixture.

4.1. Studied cases on the synthetic signal

To select a proper window length to perform all the simulations, performance and computational time are evaluated for different numbers of samples. Figures 4.1 and 4.2 show the result. The signal is built with white noise and a total SNR almost equal to 1.5. Increasing the window length, the SDR increases, leading to a more precise result, but the overall computational time increases. The increase in the computational cost is of $\mathcal{O}(N^3)$. Figures 4.3, 4.4, 4.5, and 4.6 show the outcomes for rolls 5 and 8 for different window lengths and provide a qualitative understanding of different values of SDR. Particularly, the bar plot on the top shows the amplitude values of the harmonic components of the extracted and generated signals. The plot on the bottom reports, from the top to the bottom, the entire generated signal without noise, the entire generated signal with noise, the extracted signal (red) together with the corresponding generated harmonic signal (blue) for the selected fundamental frequency, and the effect of one revolution of the roll for extracted (red) and generated (blue) harmonic patterns. Roll 8 presents a quite low performance, due to the low amplitude values of its harmonic components, therefore it is chosen as the reference to set the minimum acceptable window length.

A trade-off between accuracy and time needed for the computation is chosen and a window length of 20 s is selected for the following simulations. This window length corresponds to 20000 samples given the sampling frequency of 1000 Hz. The minimum SDR for the selected window length, which is reached with roll 8, is equal to 4.48 $\frac{1}{\mu\text{m}}$. To this SDR value corresponds an average error in the amplitude values of the harmonic components

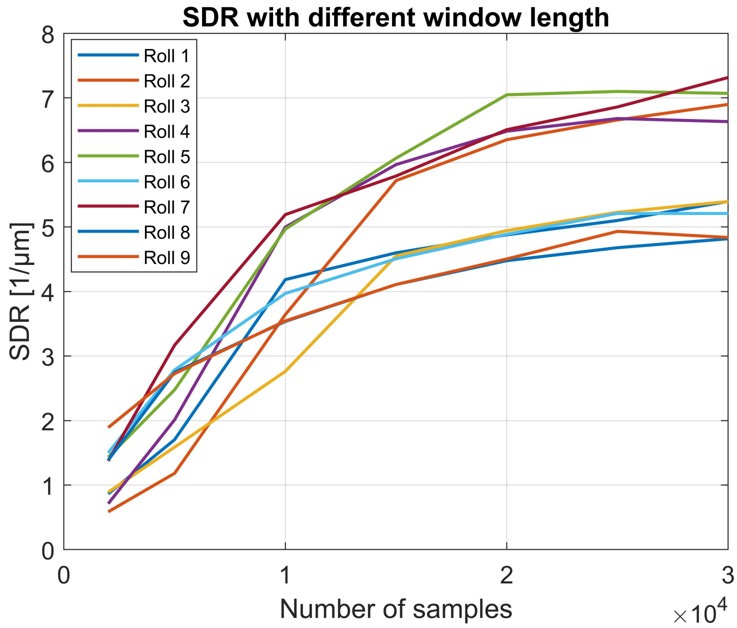

Figure 4.1: Performance evaluation through SDR for different numbers of samples when the signal is built with a sampling frequency of 1000 Hz. The outcome is shown for all 9 fundamental frequencies of the signal. The result is more accurate for higher numbers of samples presenting a steeper increment in the SDR in the left part of the graph.

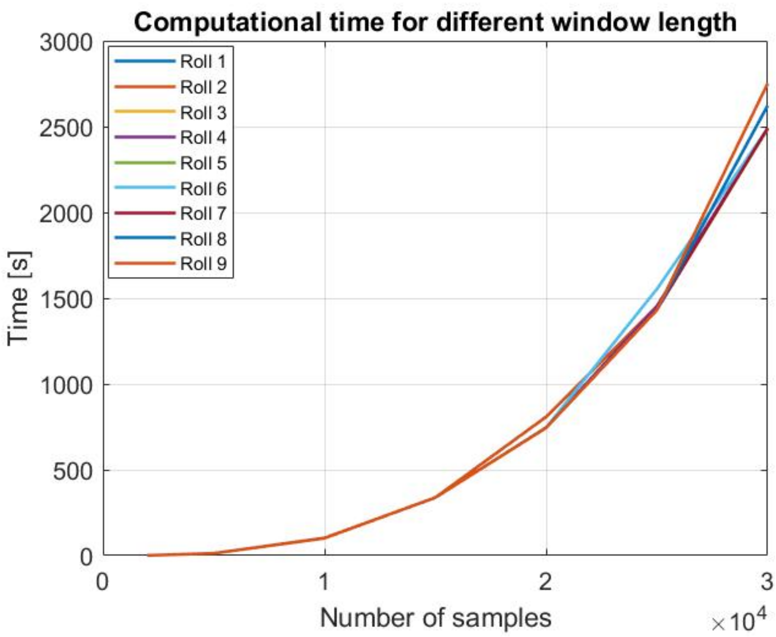

Figure 4.2: Computational time for different numbers of samples when the signal is built with a sampling frequency of 1000 Hz. The required time increases as the number of samples increases, following a cubic trend with respect to the latter.

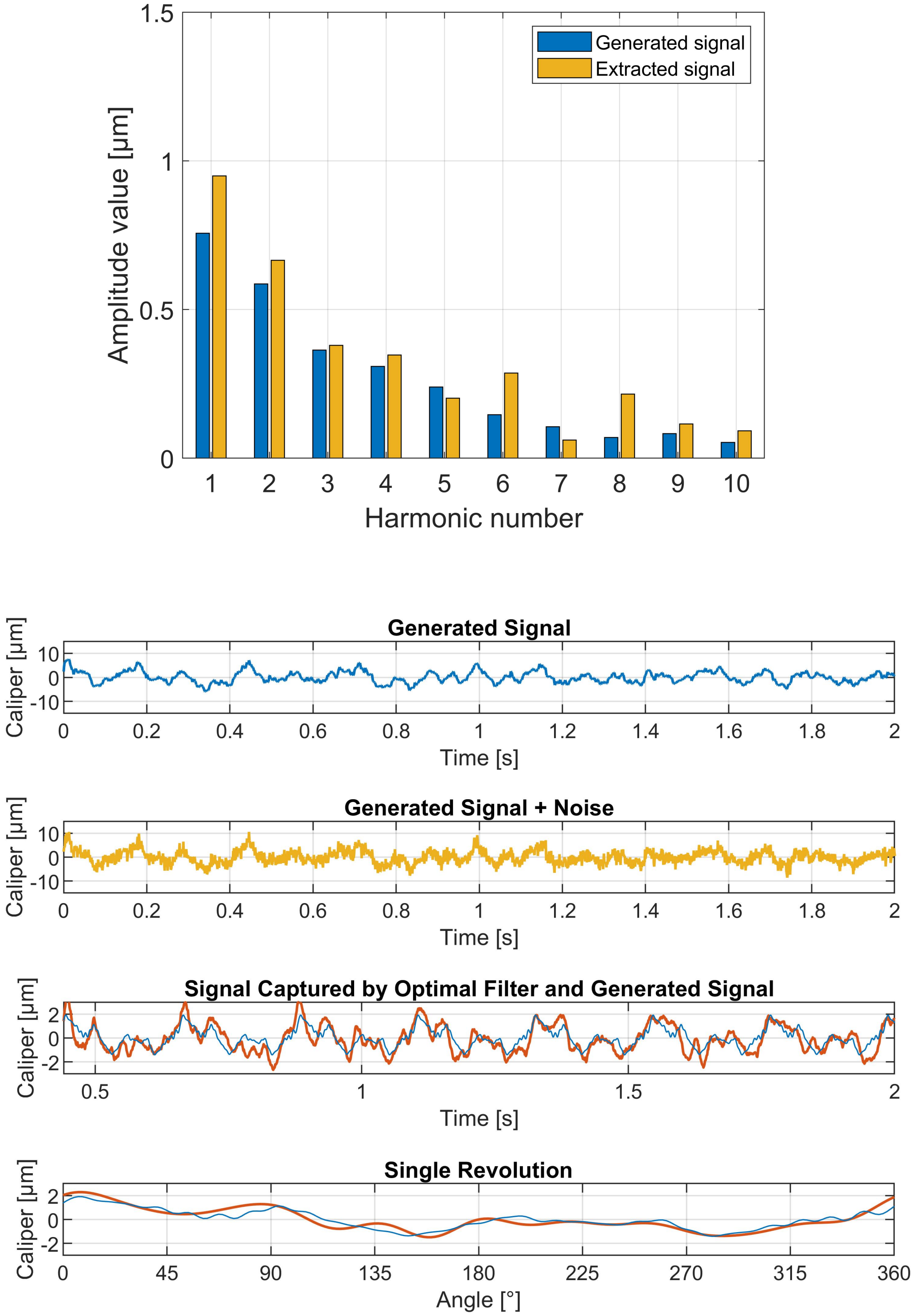

Figure 4.3: Bar plot of the amplitude values (top) and plot of generated and extracted signals in time (bottom). In the last two graphs, the generated signal (blue line) and the extracted one (red line) are plotted together. The selected frequency is equal to 4.539 Hz, which corresponds to roll 5. The window length is 2000 samples and the SDR is 1.43 $\frac{1}{\mu m}$.

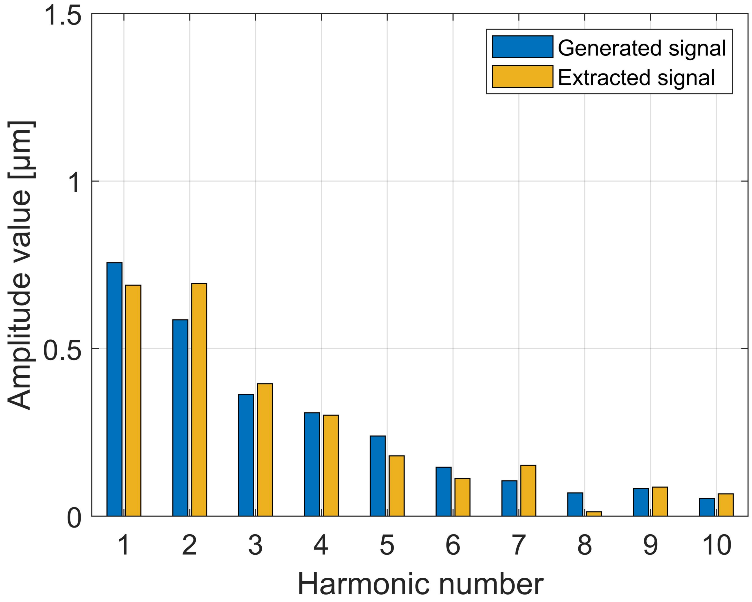

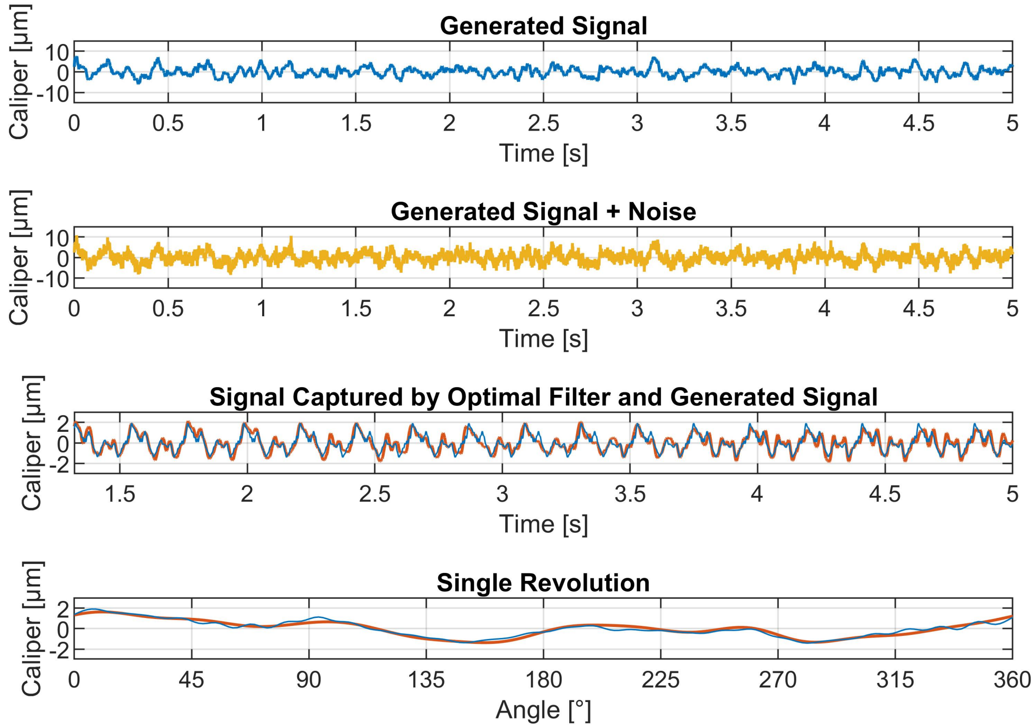

Figure 4.4: Bar plot of the amplitude values (top) and plot of generated and extracted signals in time (bottom). In the last two graphs, the generated signal (blue line) and the extracted one (red line) are plotted together. The selected frequency is equal to 4.539 Hz, which corresponds to roll 5. The window length is 5000 samples and the SDR is 2.48 $\frac{1}{\mu m}$.

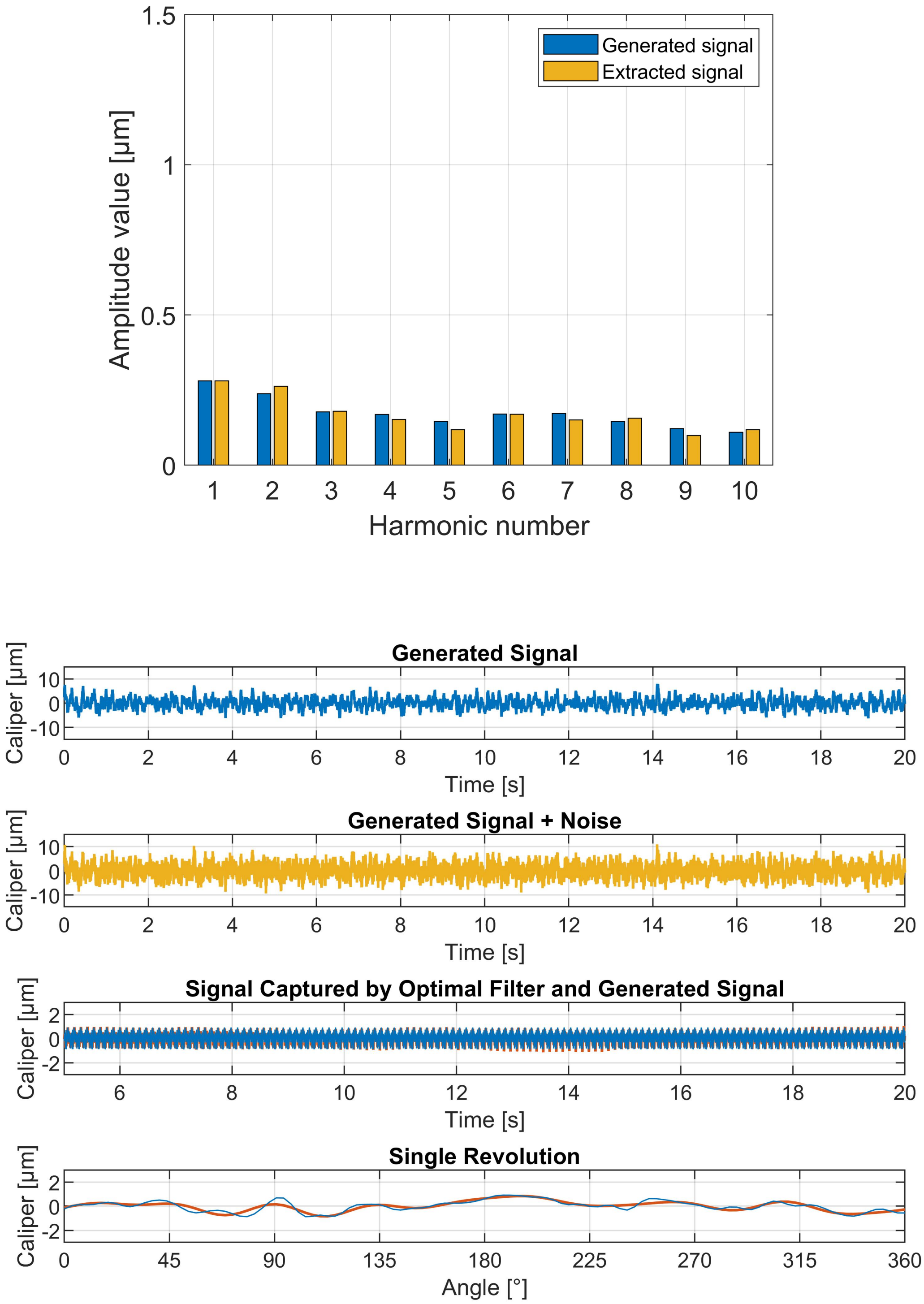

Figure 4.5: Bar plot of the amplitude values (top) and plot of generated and extracted signals in time (bottom). In the last two graphs, the generated signal (blue line) and the extracted one (red line) are plotted together. The selected frequency is equal to 8.585 Hz, which corresponds to roll 8. The window length is 20000 samples and the SDR is $4.48\frac{1}{\mu\text{m}}$.

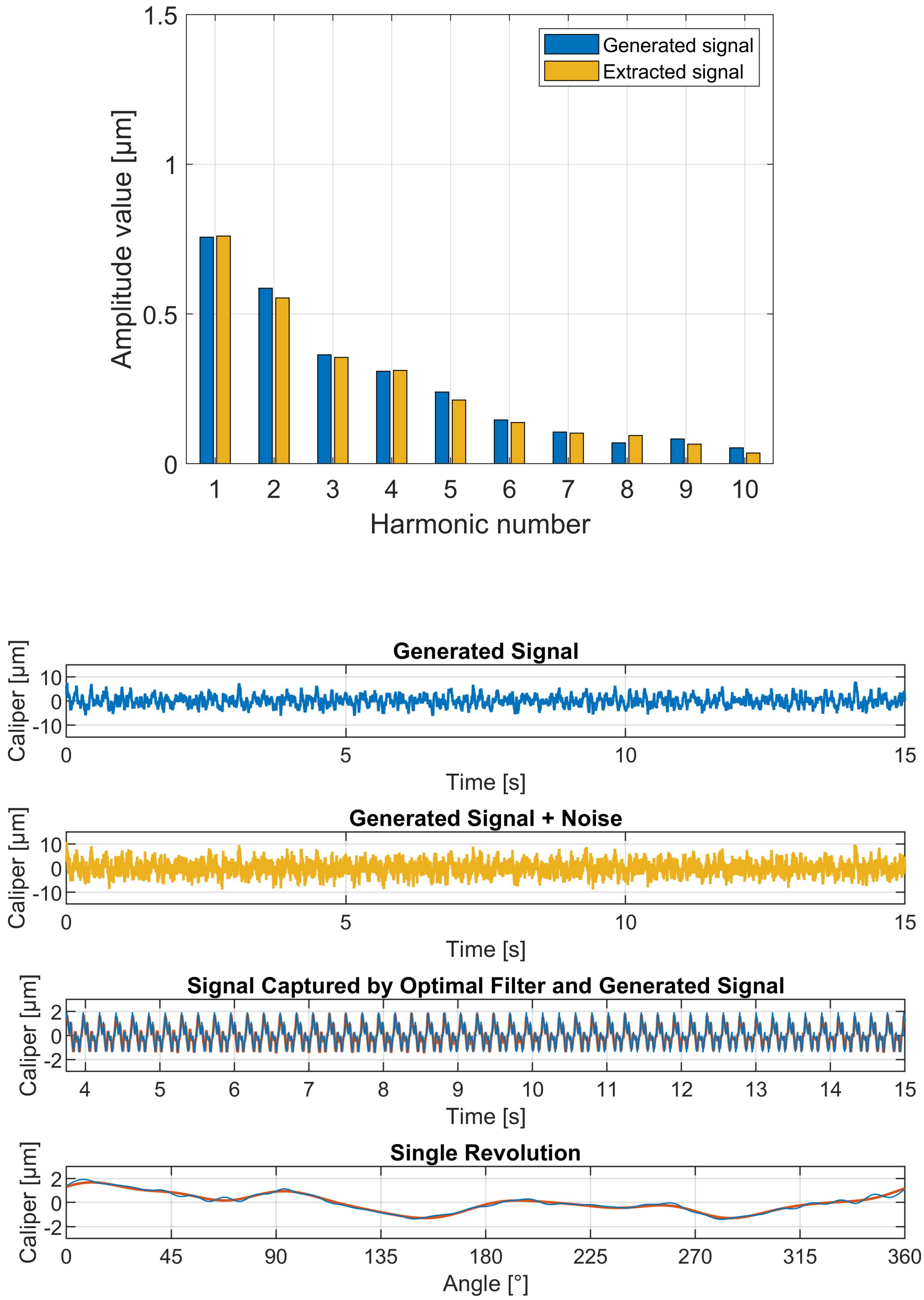

Figure 4.6: Bar plot of the amplitude values (top) and plot of generated and extracted signals in time (bottom). In the last two graphs, the generated signal (blue line) and the extracted one (red line) are plotted together. The selected frequency is equal to 4.539 Hz, which corresponds to roll 5. The window length is 15000 samples and the SDR is $6.06 \frac{1}{\mu m}$.

of 0.014 μm (Figure 4.5).

Figure 4.7 shows that with a lower sampling frequency, 700 Hz in this specific case, it is possible to obtain a good result with a lower number of samples. This suggests that the performance is more connected to the number of rotations of each roll during the acquisition time than to the number of samples itself.

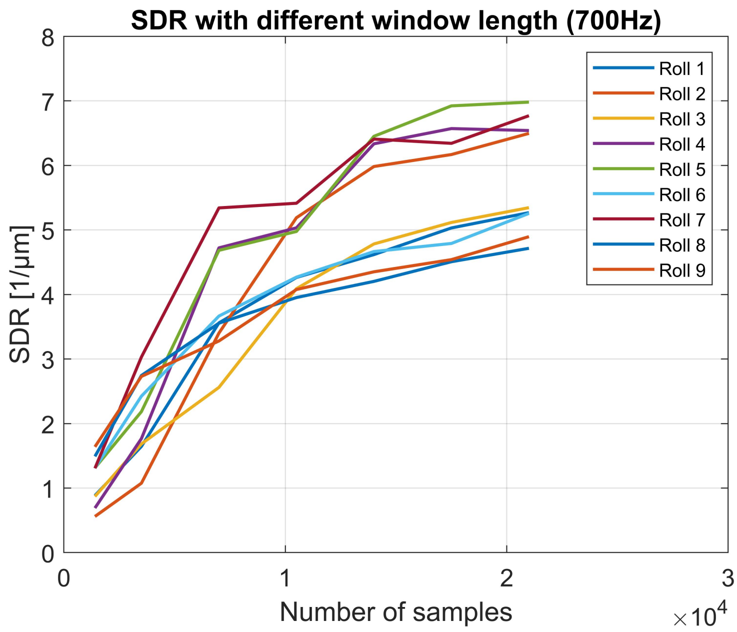

Figure 4.7: Performance evaluation through SDR for different numbers of samples when the signal is built with a sampling frequency of 700 Hz. The outcome is shown for all 9 fundamental frequencies of the signal. With this sampling frequency is possible to obtain better performance with a lower number of samples, compared to the case in which the sampling frequency is 1000 Hz.

As mentioned in the previous chapter the synthetic signal is composed of 9 harmonic series. The effect of a different number of harmonic series has been analyzed adding to the signal one harmonic series with a fundamental frequency of 1.9 Hz and one with 9 Hz. Table 4.1 reports the percentage variation of SDR computed from the nominal case, i.e. the signal with 9 harmonic series, as in Equation 4.1. The added components have a beneficial effect on some rolls, leading to an increase in the SDR, i.e. a negative variation. For other rolls, instead, the SDR decreases. This means that the added series is interfering with the extracted series, and it is hindering the extraction of the correct amplitudes of the harmonic components. This happens when the fundamental frequency of the added series or one of its multiples is close to the fundamental frequency of the extracted series or one of its multiples. The effect of the added series also depends on the amplitude values of its harmonic components, being stronger for higher amplitude values.

$$var = \frac{SDR_{nom} - SDR_{new}}{SDR_{nom}} * 100. \tag{4.1}$$

Freq [Hz]	Roll 1	Roll 2	Roll 3	Roll 4	Roll 5	Roll 6	Roll 7	Roll 8	Roll 9
1.9	-0.94	-4.98	8.35	2.22	6.02	-1.64	-2.28	-1.30	4.20
9	-2.04	-4.60	8.12	3.27	16.96	-5.43	4.39	-0.04	-9.83

Table 4.1: SDR variation caused by the presence of an additional harmonic series. The result is reported for two different values of the fundamental frequency of the added series. The SDR variation is computed from the nominal case, in which no harmonic series are added, as in Equation 4.1.

4.1.1. Extraction of a frequency not present in the signal or a series with one missing harmonic component

One of the first tests performed on the synthetic signal consists in analyzing what happens when the filter tries to extract a frequency that is not present in the signal. This test reproduces two possible realistic conditions. The first is the condition in which the roll under analysis is not impacting product quality. The second, instead, represents the condition in which the rotational frequency of the roll under analysis has deviated greatly from the set point, and therefore the filter is unable to detect it.

The same signal is analyzed with different levels of white noise. Figure 4.8 shows the relation between the RMS of the extracted signal and the RMS of the noise. The RMS of the signal approximately linearly increases with the RMS of the noise. The result is compared with the RMS of a harmonic series present in the signal. Even if the RMS of the extracted signal is not equal to zero, as it should be, it is much lower than the one of a harmonic series present in the signal.

To better compare the noise level and amplitude of the extracted harmonic components, the noise spectra and bar plots of the amplitude values are reported in Figure 4.9 for three different levels of noise. Looking at the results, it is possible to conclude that the filter is not properly able to reject the noise when it receives as input an absent frequency.

The second test, instead, studies the effect of a missing harmonic component in the signal. This is done by removing one harmonic component at a time from the harmonic series

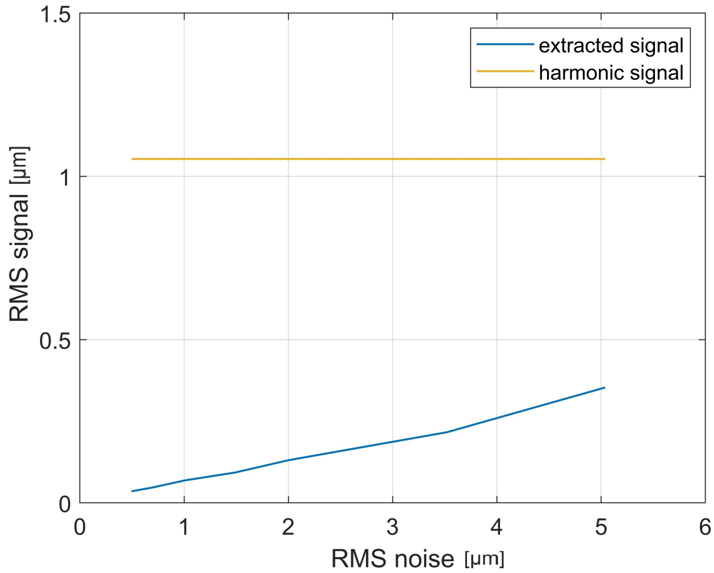

Figure 4.8: RMS of the extracted signal (blue) when the filter input frequency is not present in the signal. The result is plotted as a function of the RMS of the noise of the signal and it almost follows a linear increasing behavior. The RMS of the extracted signal is compared with the RMS of a harmonic series of the signal.

corresponding to the second roll, i.e. the roll with a rotational frequency of 2.352 Hz, and computing the SDR of the extracted signal. As it is possible to verify from Figure 4.10 the result is the same for all the missing harmonic components. The results are compared with the nominal case, in which all the harmonic components are present, by computing the SDR variation as in Equation 4.1. The variation is bounded in the interval [-6% - +6%] showing that the effect of a missing harmonic has no relevant impact. The noise spectra and amplitude values of the extracted signal are shown in Figure 4.11 for three tests done with different levels of noise and different missing harmonic numbers.

4.1.2. Different noise amplitudes

Since no exact information about the noise present in the machine environment is available, tests with different types and levels of noise are performed. First, a signal with white noise is considered, in agreement with the hypothesis of the filter. The amplitude of the noise is varied to understand the SNR the filter can deal with. Since, as previously stated from the analysis of the PSDs of the signals (Figure 3.6), the noise probably presents a higher energy content at lower frequencies, a signal with pink noise is also examined. Figure 4.12 shows the result in terms of SDR for the two types of noise and different values of SNR. As expected, the lower the SNR, i.e. the higher the noise level, the lower

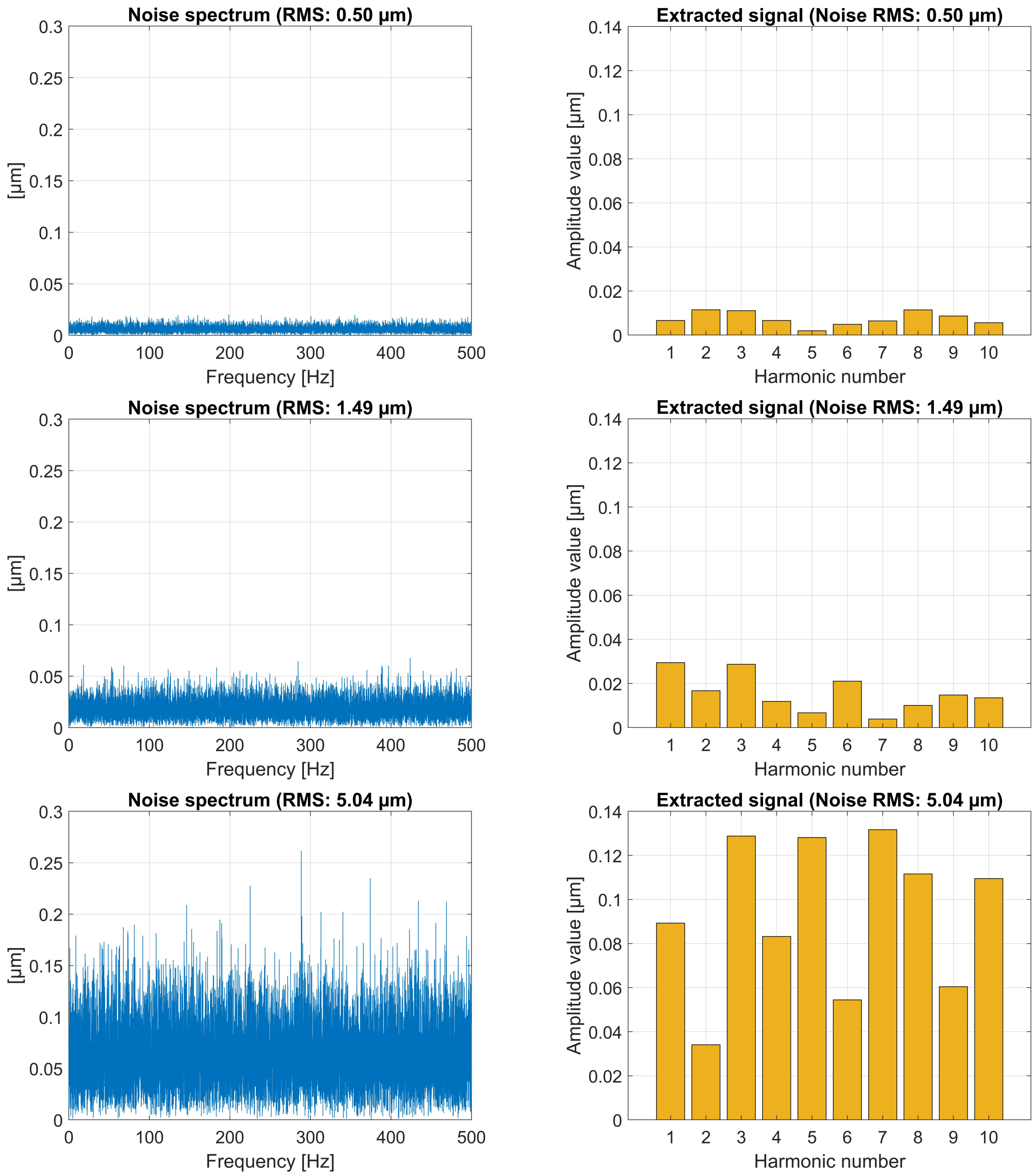

Figure 4.9: Noise spectrum (left) and amplitude values of the harmonic components of the extracted signal (right) for different noise amplitudes. The extracted frequency is not present in the signal. In all the cases the extracted amplitude values are not null, therefore the filter is not able to completely reject the noise.

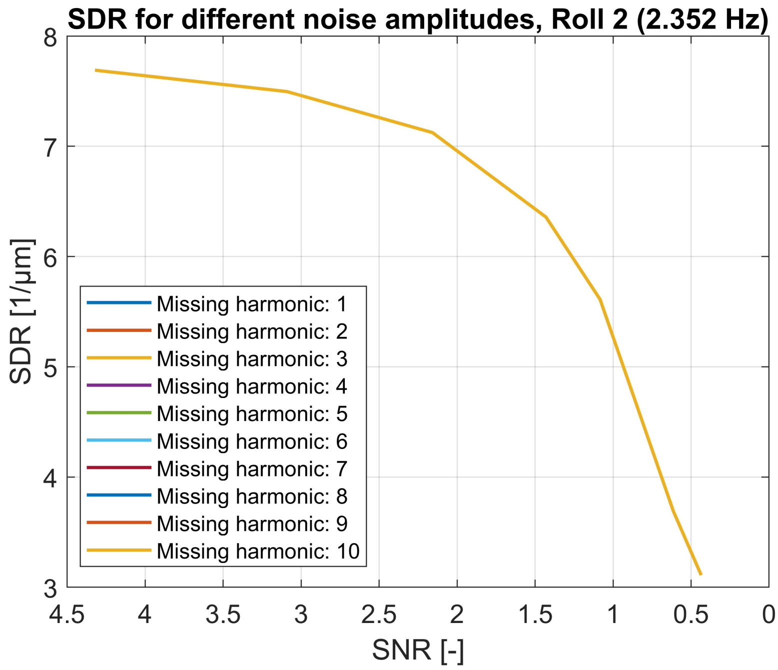

Figure 4.10: SDR computed for different SNRs and different missing harmonics from the generated signal. The roll analyzed is the one with a rotational frequency of 2.352 Hz (roll 2). The number of the missing harmonic component has no impact on the performance that decreases increasing the noise level.

the performance. In presence of pink noise, the filter is still able to provide a good result, but for higher SNRs compared to the case of white noise. In addition, the presence of pink noise mainly affects the rolls with a lower rotational frequency. This is also expected since the pink noise has a higher energy content at lower frequencies.

4.1.3. Wrong input frequency

As described before, the frequency of variation can slightly differ from the set point of the roll rotational frequency. To simulate this condition, a wrong frequency is given as input to the filter. The input frequency ω_{in} is computed by considering a percentage error from the right frequency ω_0 as

$$\omega_{in} = \frac{error}{100} * \omega_0 + \omega_0. \tag{4.2}$$

The SDR is computed for all the different rolls considering error values from 0% to 0.5%. Figure 4.13 shows the result in the case of white noise with a total SNR almost equal to 1.5. The same figure shows how the performance is improved with a frequency detection performed before the extraction of the filtered signal. Figure 4.14 reports the result of the same test done with a signal with pink noise and an SNR approximately equal to

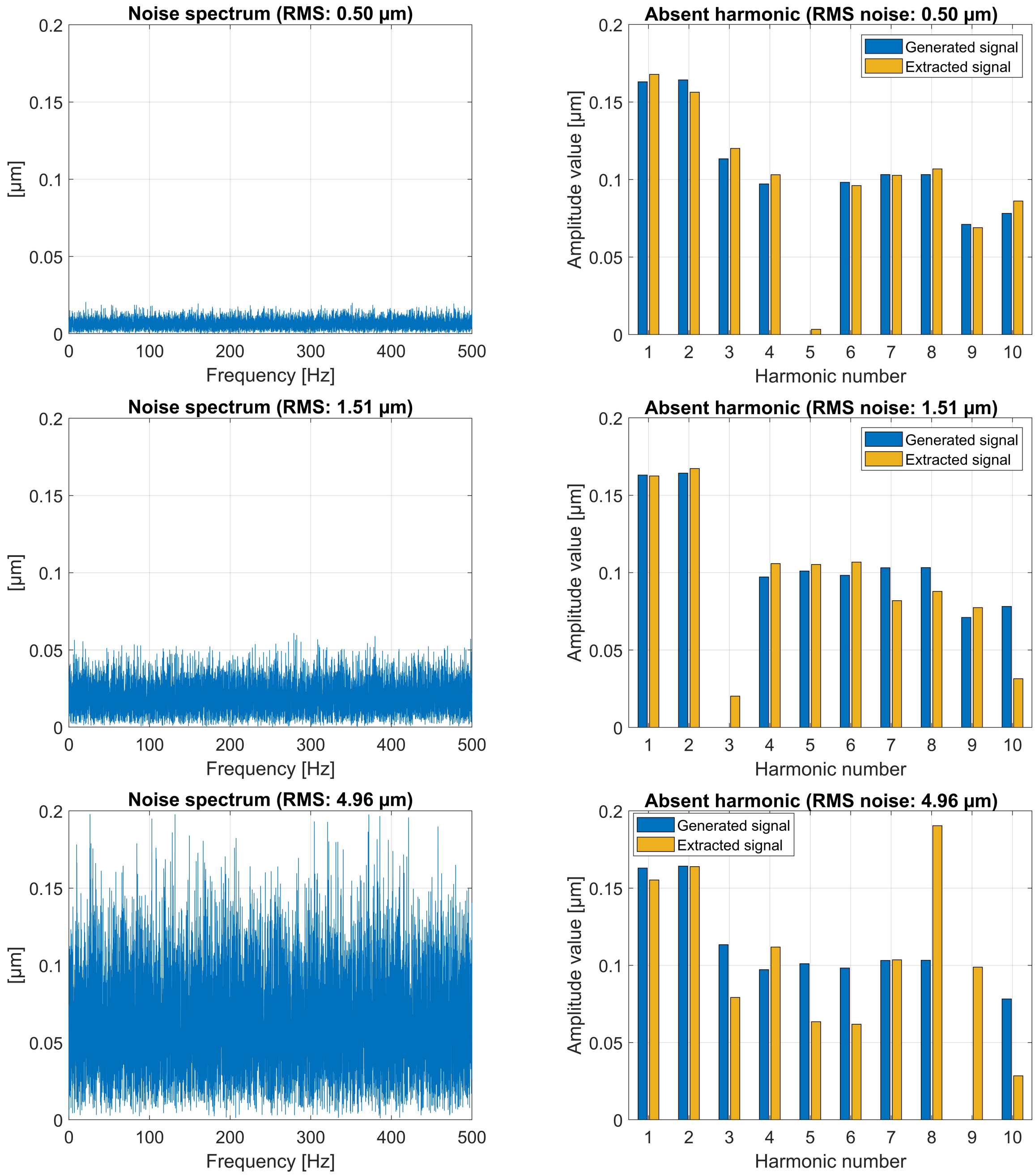

Figure 4.11: Noise spectrum (left) and amplitude values of the harmonic components of extracted and generated signals (right) for different noise amplitudes. The frequency extracted is the one that corresponds to the second roll. In the three cases, different harmonic components are canceled from the signal. The higher the noise level the higher the amplitude of the extracted missing harmonic.

2.5. To better visualize the results, tables 4.2 and 4.4 report the SDR variation from the nominal case, where the input frequency is the correct one, in presence of white and pink noise without frequency detection. Since the error is defined as a percentage

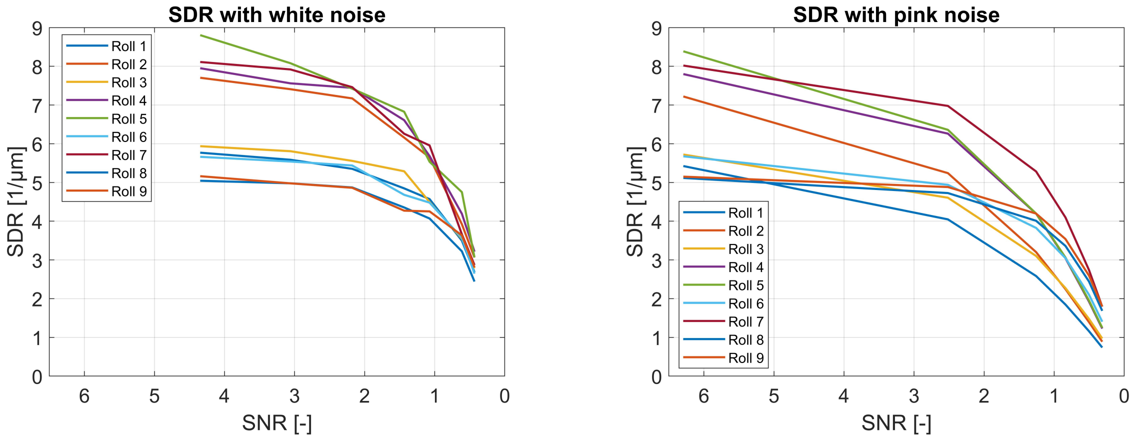

Figure 4.12: SDR computed for different white (left) and pink (right) noise amplitudes. In both cases, the performance decreases for lower SNRs, i.e. higher noise levels. For the same SNR values, performance is higher in presence of white noise.

of the correct frequency, the higher frequencies are more affected by it. In the case of pink noise, the variation in SDR for the lower frequencies is lower compared to the case of white noise. This is probably because the high noise at low frequency has a higher contribution to the performance than the error in the input frequency. Tables 4.3 and 4.5 report the variation in the SDR parameter obtained with frequency detection. Overall, the performance is improved, except for some cases at low frequency and with a low error. Increasing the resolution of the frequency detection is sufficient to overcome this problem. However, this implies a higher computational burden.

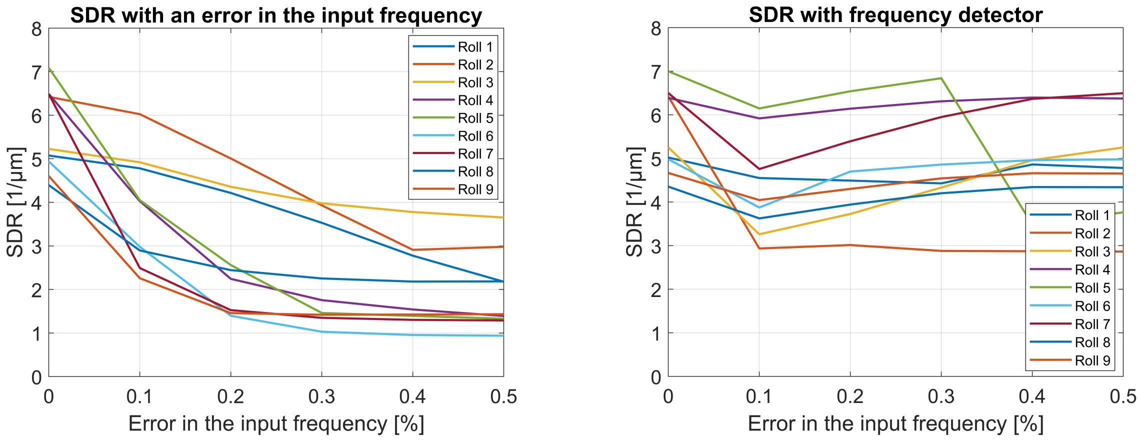

Figure 4.13: SDR computed considering an error in the filter input frequency without (left) and with (right) frequency detection. The SDR is plotted as a function of the error in the input frequency. The signal is built with white noise and a total SNR approximately equal to 1.5.

Roll n.	**0.0%**	**0.1%**	**0.2%**	**0.3%**	**0.4%**	**0.5%**
1	0.00	5.78	16.93	30.43	45.30	57.09
2	0.00	6.20	22.04	38.78	54.69	53.61
3	0.00	5.86	16.62	23.88	27.71	30.12
4	0.00	37.91	65.42	72.94	76.25	78.56
5	0.00	42.86	63.88	79.39	80.34	81.26
6	0.00	39.67	71.73	79.15	80.66	80.99
7	0.00	61.57	76.48	79.19	79.91	80.12
8	0.00	34.12	44.39	48.73	50.36	50.26
9	0.00	50.95	68.33	69.16	69.04	68.89

Table 4.2: SDR variation computed from the nominal case, in which the input frequency is the correct one. The variation is computed as in Equation 4.1 for different errors in the input frequency. The error is expressed as a percentage of the correct frequency and ranges from 0 to 0.5%. The signal is built with white noise and a total SNR almost equal to 1.5.

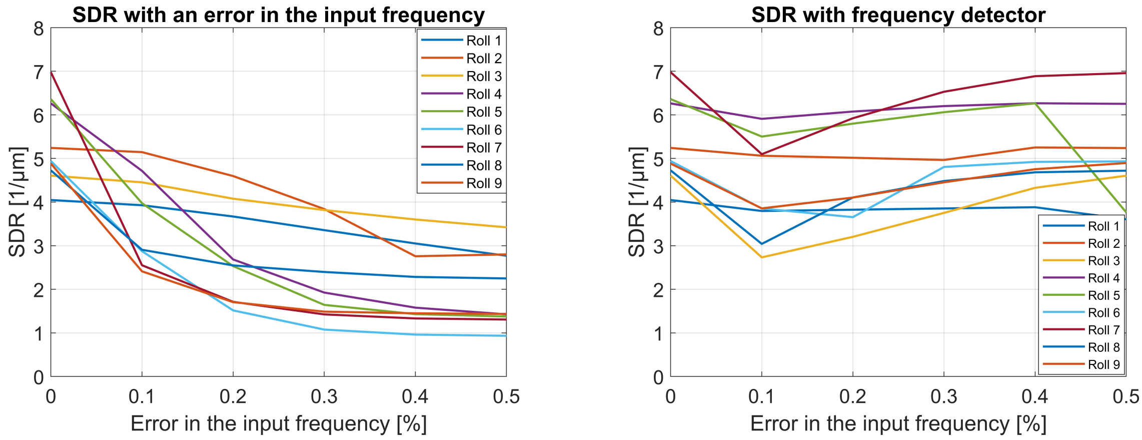

Figure 4.14: SDR computed considering an error in the filter input frequency without (left) and with (right) frequency detection. The SDR is plotted as a function of the error in the input frequency. The signal is built with pink noise and a total SNR approximately equal to 2.5.

Roll n.	**0.0%**	**0.1%**	**0.2%**	**0.3%**	**0.4%**	**0.5%**
1	0.00	9.35	10.53	11.78	3.16	4.76
2	0.00	54.28	53.06	55.15	55.27	55.38
3	0.00	37.92	29.05	17.52	5.58	0.00
4	0.00	7.35	3.87	1.22	-0.12	0.22
5	0.00	12.18	6.54	2.27	50.20	46.21
6	0.00	22.22	5.68	2.47	0.45	0.08
7	0.00	26.80	17.01	8.45	2.05	0.04
8	0.00	16.75	9.46	3.49	0.23	0.31
9	0.00	13.32	7.82	2.66	0.13	0.26

Table 4.3: SDR variation computed from the nominal case, in which the input frequency is the correct one. The variation is computed as in Equation 4.1 for different errors in the input frequency. The error is expressed as a percentage of the correct frequency and ranges from 0 to 0.5%. The signal is built with white noise and a total SNR almost equal to 1.5. A frequency detection is applied.

Roll n.	**0.0%**	**0.1%**	**0.2%**	**0.3%**	**0.4%**	**0.5%**
1	0.00	2.95	9.34	17.07	24.63	31.57
2	0.00	1.84	12.30	26.74	47.39	46.58
3	0.00	3.32	11.48	17.13	21.83	25.73
4	0.00	24.69	57.14	69.26	74.78	77.23
5	0.00	37.51	60.20	74.17	77.49	78.36
6	0.00	41.83	69.31	78.21	80.53	81.08
7	0.00	63.44	75.46	79.58	80.91	81.27
8	0.00	38.52	46.10	49.28	51.68	52.42
9	0.00	50.62	65.08	69.53	70.31	70.58

Table 4.4: SDR variation computed from the nominal case, in which the input frequency is the correct one. The variation is computed as in Equation 4.1 for different errors in the input frequency. The error is expressed as a percentage of the correct frequency and ranges from 0 to 0.5%. The signal is built with pink noise and a total SNR approximately equal to 2.5.

Roll n.	**0.0%**	**0.1%**	**0.2%**	**0.3%**	**0.4%**	**0.5%**
1	0.00	6.22	5.49	4.78	4.09	10.91
2	0.00	3.42	4.31	5.28	-0.20	0.07
3	0.00	40.68	30.46	18.54	6.06	0.03
4	0.00	5.65	2.98	0.98	-0.06	0.16
5	0.00	13.49	8.82	4.69	1.52	40.83
6	0.00	22.01	26.02	2.72	0.37	0.14
7	0.00	26.94	15.12	6.41	1.29	0.29
8	0.00	35.66	13.15	5.17	0.93	0.15
9	0.00	21.04	15.96	8.79	2.63	-0.26

Table 4.5: SDR variation computed from the nominal case, in which the input frequency is the correct one. The variation is computed as in Equation 4.1 for different errors in the input frequency. The error is expressed as a percentage of the correct frequency and ranges from 0 to 0.5%. The signal is built with pink noise and a total SNR approximately equal to 2.5. A frequency detection is applied.

4.1.4. Presence of two close frequencies in the signal

An additional test executed with the synthetic signal consists in adding a harmonic series with a fundamental frequency close to one of the frequencies present in the signal. The

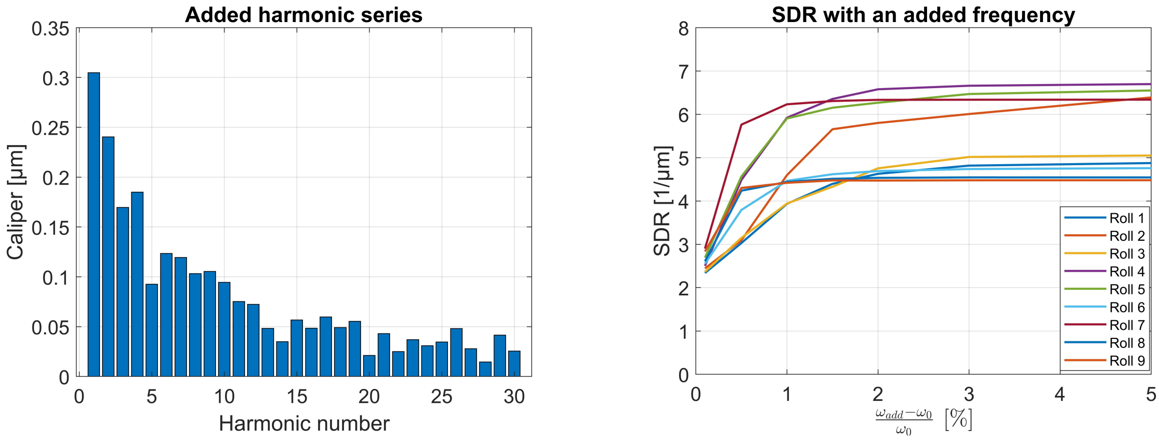

Figure 4.15: Amplitude values of the added harmonic series (left) and SDR computed for different values of the fundamental frequency of the added series (right). The SDR is plotted as a function of the difference between the added frequency and the extracted frequency normalized over the latter. The closer the two frequencies the lower the performance. The signal is built with white noise and a total SNR almost equal to 1.5.

added frequency is defined such that

$$\frac{\omega_{add} - \omega_0}{\omega_0} \quad \in \quad [0.1\% - 5\%]. \tag{4.3}$$

The test is done for all 9 fundamental frequencies of the signal, and it is useful to understand when a filter can distinguish two frequencies and when, instead, they are too close to be separated. Figure 4.15 shows the amplitude values of the harmonic components of the added harmonic series and the result in terms of performance obtained in the case of white noise with an SNR around 1.5. The lower the difference between the frequency of the added series and the extracted one the lower the performance. Table 4.6 presents the percentage variation of SDR from the case in which no frequency is added. The rolls with a higher rotational frequency are less affected by the added frequency. This is clear since the added frequency is defined as a percentage of the frequency of the signal.

Roll n.	0.10%	0.50%	1%	1.50%	2%	3%	5%
1	51.75	37.50	18.85	9.33	4.55	0.66	-0.56
2	60.30	49.80	25.37	8.17	5.82	2.48	-3.73
3	55.25	40.45	25.49	18.16	10.13	5.18	4.54
4	62.14	32.13	10.40	3.86	0.48	-0.76	-1.33
5	60.56	33.14	13.53	9.89	8.20	5.26	4.06
6	45.48	18.98	4.64	1.38	-0.18	-1.18	-1.63
7	53.65	7.94	0.44	-0.76	-1.19	-1.24	-1.27
8	40.12	2.69	-1.93	-3.61	-4.11	-4.34	-4.33
9	33.65	-0.66	-3.45	-4.74	-4.67	-4.80	-4.84

Table 4.6: SDR variation computed from the nominal case, in which the harmonic series is not added. The difference between the added frequency and the extracted frequency is normalized over the latter and expressed in percentage. The variation is computed as in Equation 4.1. The signal is built with white noise and a total SNR almost equal to 1.5.

The same test is performed on a signal with pink noise. Table 4.7 shows the SDR variation that is computed as before. From the results, it is possible to notice that the method can handle worse the presence of two close frequencies in this case.

Roll n.	0.10%	0.50%	1%	1.50%	2%	3%	5%
1	47.79	40.38	30.62	23.34	17.45	10.96	3.25
2	56.35	52.60	42.79	29.12	19.94	14.80	4.45
3	48.66	36.20	27.41	19.88	8.68	1.71	-0.04
4	60.26	43.26	24.08	15.35	7.13	2.28	0.21
5	58.58	38.84	16.16	9.80	7.00	2.23	1.03
6	48.12	23.88	9.81	4.98	2.24	0.56	0.02
7	56.43	15.86	3.76	1.11	0.09	0.02	0.02
8	46.56	11.13	4.00	1.21	0.37	0.00	0.05
9	35.60	5.72	0.76	0.11	0.05	0.02	0.01

Table 4.7: SDR variation computed from the nominal case, in which the harmonic series is not added. The difference between the added frequency and the extracted frequency is normalized over the latter and expressed in percentage. The variation is computed as in Equation 4.1. The signal is built with pink noise and a total SNR approximately equal to 2.5.

4.1.5. Non-stationary signal

The filter theoretically requires as input a stationary signal. However, the acquired signal can present some non-stationarities, for example, a change of frequency or noise. In this thesis, two tests are reported. In the first one, the filter is applied to a chirp signal, i.e. a signal characterized by a linearly increasing value of frequency in time. In the second test, the signal is subjected to a sudden rise in the noise level, occurring in the first M samples. Figure 4.16 reports the SDR value for chirp signals with both white and pink noise. The frequency variation on the x-axis denotes the percentage variation between the initial and the final frequencies of the chirp signal, normalized over the initial frequency. Even in this case, the decrease in performance is less pronounced for the lower frequencies since the variation is computed as a percentage of the initial frequency. The decreasing behavior is similar between the two cases, showing that the type of noise has no significant impact on the decrease in performance due to the presence of a non-stationarity in the harmonic signal.

To reproduce a non-stationary behavior of the noise, the noise amplitude is suddenly increased after a certain number of samples. In particular, the change occurs within the filter length M. As it is possible to see from Figure 4.17, in the case of white noise, the performance almost linearly decreases increasing the RMS variation of the noise. In presence of pink noise, instead, the trend of the SDR parameter is more similar to a decreasing exponential function. In both cases, the final SDR is mainly dependent on the final amplitude of the noise being the result very similar to the one obtained using a signal with the same amplitude of noise for the entire window length. This means that the non-stationarity does not have a significant effect on the result, and it does not contribute much to decreasing the performance.

4.2. Real data analysis

After all the simulations on the synthetic signal, the filter is also applied to real data. The set of data available includes signals of caliper, basis weight, and moisture acquired with the QCS, and signals of caliper and basis weight acquired with the Tapio analyzer. The purpose of this analysis is to derive the impact of each roll on these quality parameters and list the rolls according to how much they are affecting the quality. The influence of each roll on the quality variation is estimated by computing the RMS of the signal obtained by applying the filter to the original signal, considering an input frequency equal to the rotational frequency of the roll under investigation; the higher the RMS of the output signal the higher the impact of the roll.

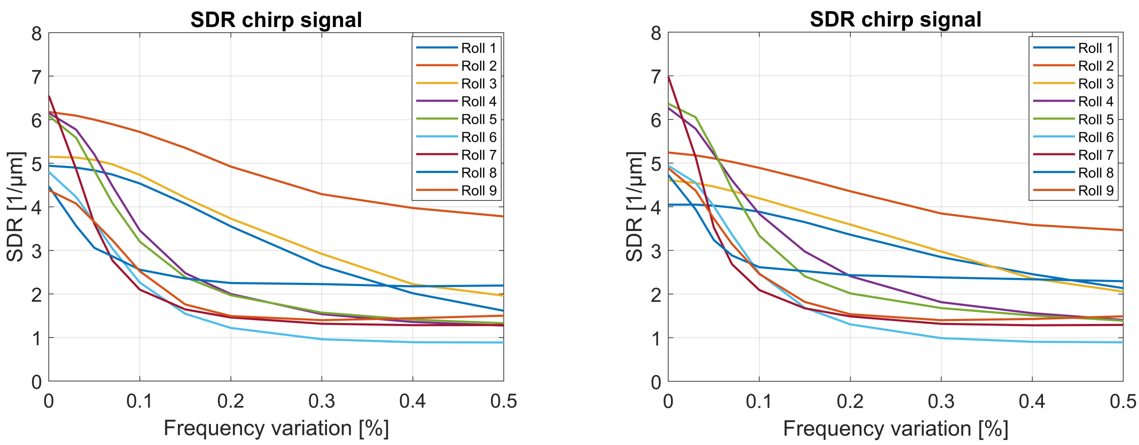

Figure 4.16: SDR computed in presence of a chirp signal for different frequency variations. The frequency variation is computed as the difference between the final and the initial frequencies of the signal, normalized over the initial one. The results are evaluated for white noise (left) and pink noise (right).

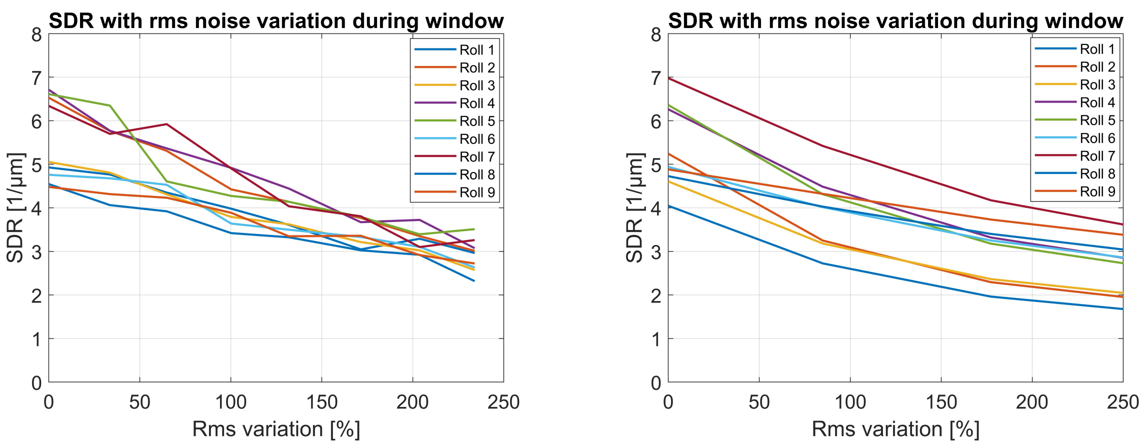

Figure 4.17: SDR computed in presence of a sudden increase in the noise level during the filter length M. The RMS variation is computed as the difference between the final and the initial RMS of the noise in the signal, normalized over the initial value of RMS. The results are evaluated for white noise (left) and pink noise (right).

Signals from QCS are characterized by a sampling frequency of 25 Hz. From the spectrum of the caliper signal in Figure 4.18, two distinct peaks can be identified at frequencies 2.35 and 4.5 Hz. Both are close to the rotational frequencies of two rolls in the machine, rolls 7 and 22 respectively. It is expected that these are the two rolls with the major impact on quality. However, the output signal obtained by applying the filter with an input frequency equal to the rotational frequency of roll 22 is not one of the signals with the highest RMS.

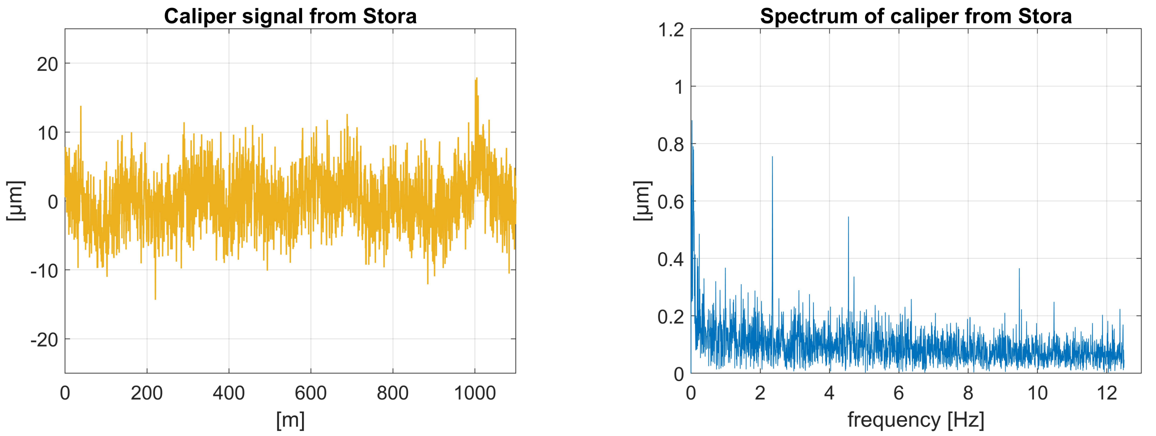

Figure 4.18: Signal and spectrum of the caliper data acquired online with the QCS on the running machine for 1.1 km of paperboard.

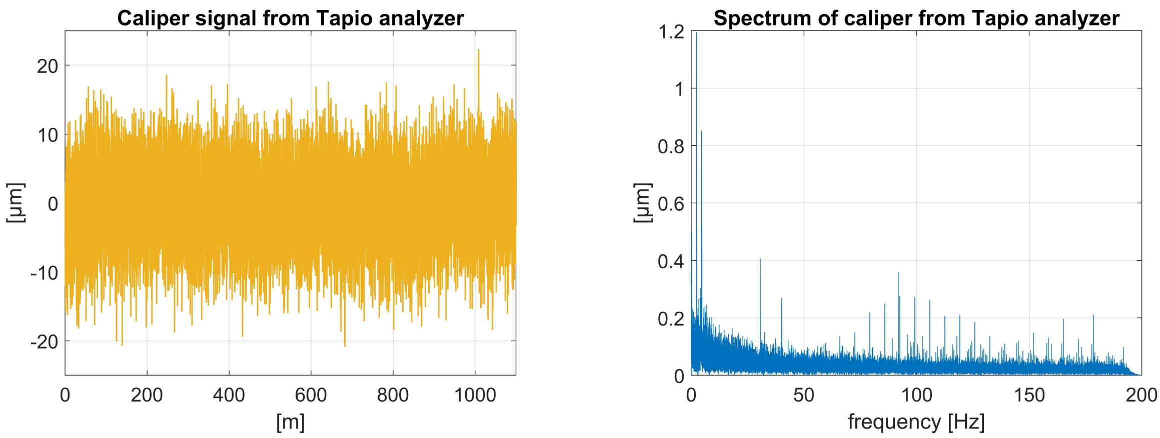

Figure 4.19: Signal and spectrum of the caliper data acquired offline with the Tapio analyzer for 1.1 km of paperboard.

The same procedure is applied to the caliper signal from the Tapio analyzer (Figure 4.19), which is characterized by a higher sampling frequency and a higher number of samples. Since the signal is very long only the first 17000 samples are used. The five rolls with the highest impact on quality are listed in Table 4.8. As expected from the spectrum of the signal, rolls 7 and 22 are the ones having the highest impact. Since the signals acquired online and offline refer to the same strip of cardboard, they should have the same outcome. It is therefore reasonable to think that the result obtained with the QCS data is not correct. This is probably due to the very low sampling frequency and the low number of samples. For this reason, the results obtained by applying the filter to the QCS data are deemed to be of no relevance and, therefore, are not reported.

The filter is applied as well to basis weight data (signal and spectrum in Figure 4.20). As for caliper variation, rolls are listed in Table 4.9 in order from higher to lower RMS of the output signal. Moisture data are not analyzed since data related to this parameter were not available from offline measurements.

Roll	**Rotational freq. [Hz]**	**RMS [µm]**
Thermo roll in valzone calender	2.352	1.328
Deflection-compensated calender roll	4.539	1.084
Forming roll in the body wire	2.439	0.833
Press 1 pick-up driving roll	3.730	0.819
Back wire driving/pulling roll	3.094	0.777

Table 4.8: Rolls with the highest impact on caliper variation. The higher the RMS of the extracted signal the stronger the impact of the roll.

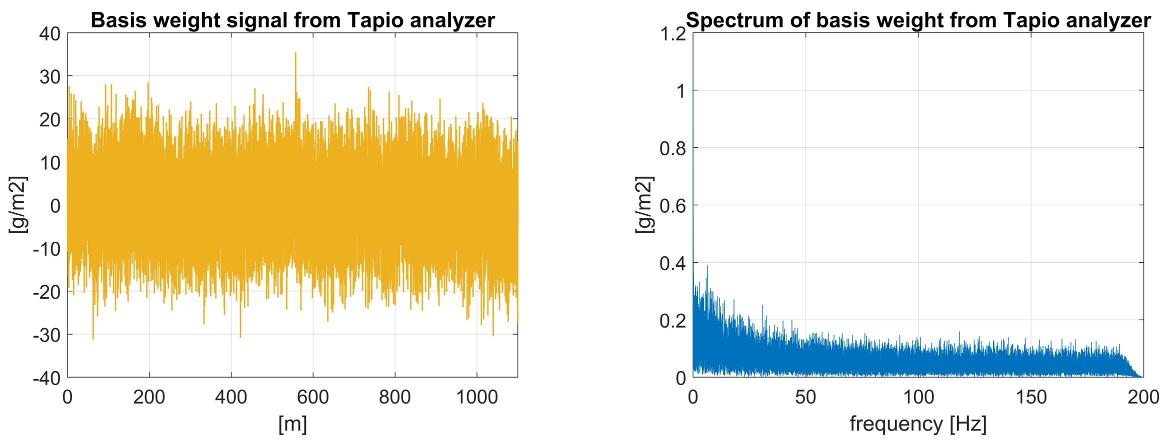

Figure 4.20: Signal and spectrum of the basis weight data acquired offline with the Tapio analyzer for 1.1 km of paperboard.

Roll	Rotational freq. [Hz]	RMS [g/m²]
Forming roll in the body wire	2.439	1.210
Surface wire joining roll	2.964	1.204
Press 1 pick-up driving roll	3.730	1.191
Back wire driving/pulling roll	3.094	1.188
Thermo roll in valzone calender	2.352	1.156

Table 4.9: Rolls with the highest impact on basis weight variation. The higher the RMS of the extracted signal the stronger the impact of the roll.

As an example, Figures 4.21 and 4.22 show the effect of roll 7, the thermo roll in the calender section, on caliper and basis weight variations. The calender section is one of the last stages of paper production. In this section some surface properties are refined, the most important of which are smoothness and gloss. The improvements of these properties lead to a loss of bulk. The figures report the caliper and basis weight signals in time together with the extracted signals having a fundamental frequency equal to the rotational frequency of the thermo roll. The figures also show the extracted amplitude values for each harmonic component and the extracted signal cut to see the effect of one rotation. Only the first 10 harmonic components are extracted, being the most significant. The higher components, indeed, have lower amplitude values. The high amplitude of the first harmonic component in Figure 4.21 indicates that the caliper variation is mainly caused by defects occurring once per revolution, probably a roll deflection. In Figure 4.22, instead, there is no dominant component.

In Figures 4.23 and 4.24 other two examples are reported. Even in these cases, the first harmonic component is the one with the highest amplitude value and the amplitude values decrease increasing the harmonic number.

4.3. SOS comparison

As the last step of this study, a comparison with the SOS tool of the Tapio analyzer is performed. The SOS analysis can extract the effect of the machine components affecting the quality the most from the signal acquired by the analyzer. Figure 4.25 shows the software interface. The analysis reports the spectrum of the signal, highlighting the frequency components connected to the element of the machine of interest, the signal in time together with the extracted signal in time, and the roundness profile of the component causing the variation.

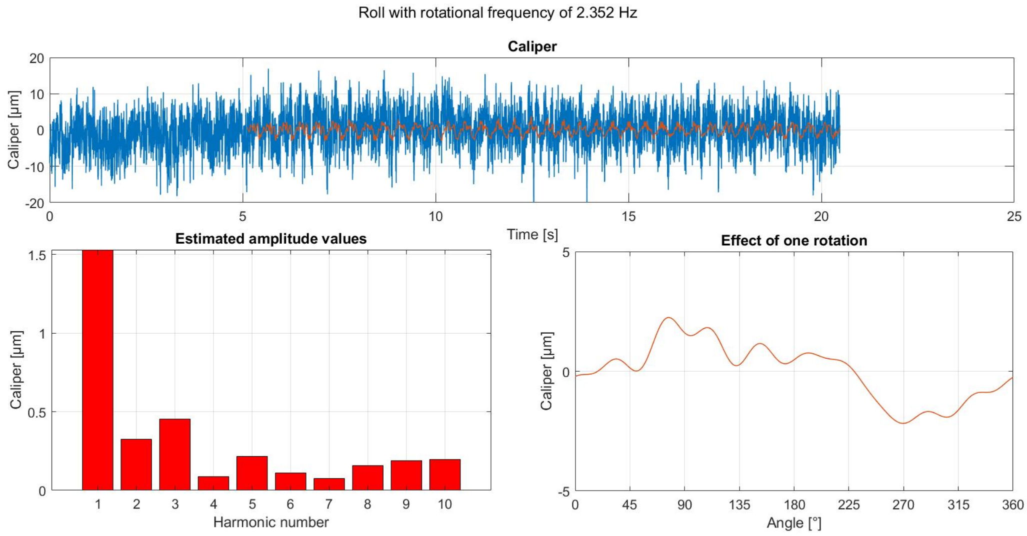

Figure 4.21: Impact of roll 7 on the caliper variation. The top figure shows the caliper signal (blue) together with the signal extracted by the filter (red). The bottom figures show the amplitude values of the extracted harmonic series and the effect on caliper of one revolution of the roll.

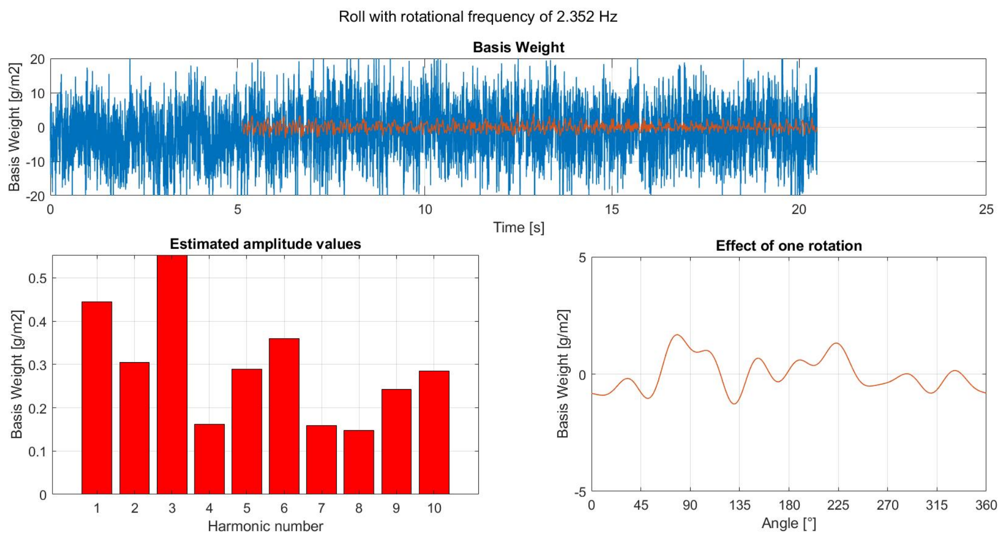

Figure 4.22: Impact of roll 7 on the basis weight variation. The top figure shows the basis weight signal (blue) together with the signal extracted by the filter (red). The bottom figures show the amplitude values of the extracted harmonic series and the effect on basis weight of one revolution of the roll.

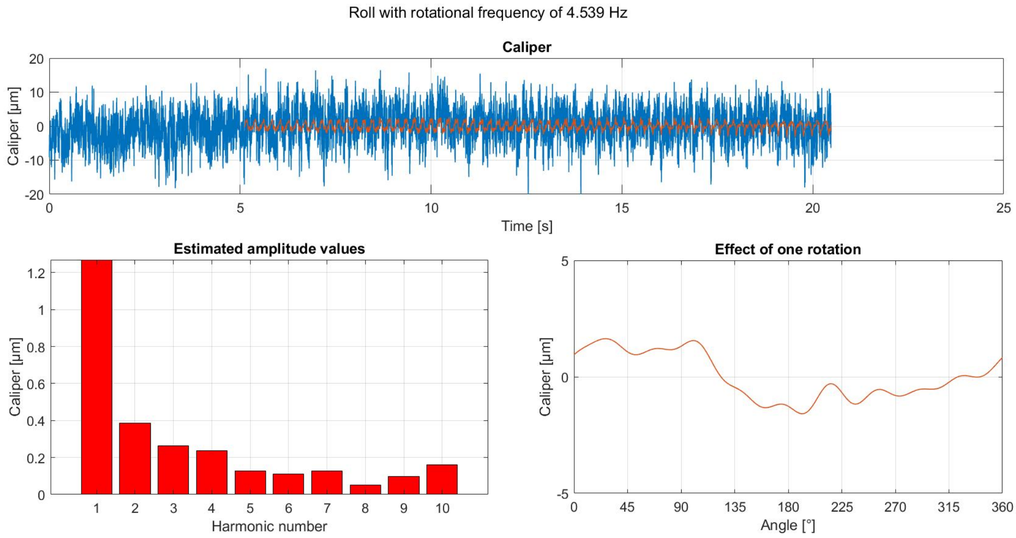

Figure 4.23: Impact of roll 22 on the caliper variation. The top figure shows the caliper signal (blue) together with the signal extracted by the filter (red). The bottom figures show the amplitude values of the extracted harmonic series and the effect on caliper of one revolution of the roll.

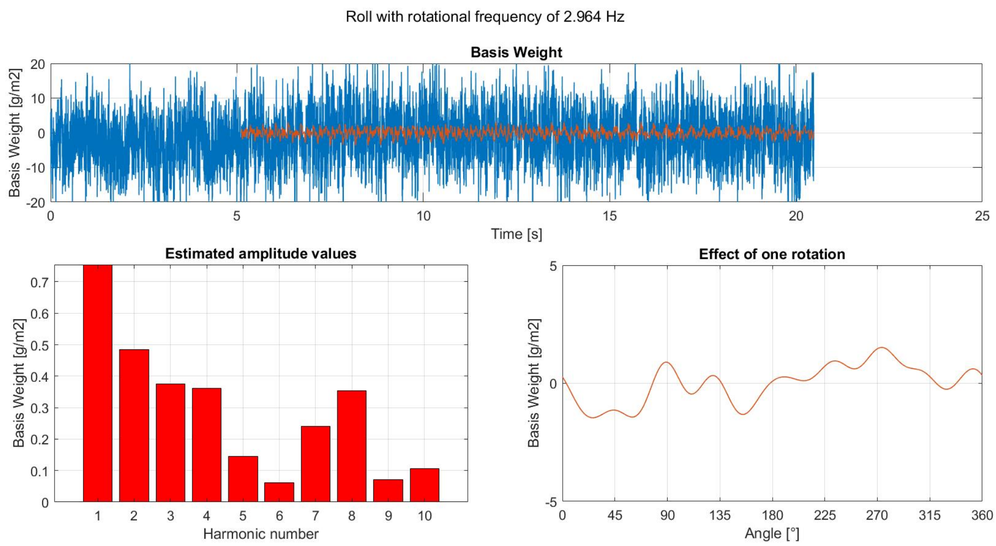

Figure 4.24: Impact of roll 12 on the basis weight variation. The top figure shows the basis weight signal (blue) together with the signal extracted by the filter (red). The bottom figures show the amplitude values of the extracted harmonic series and the effect on basis weight of one revolution of the roll.

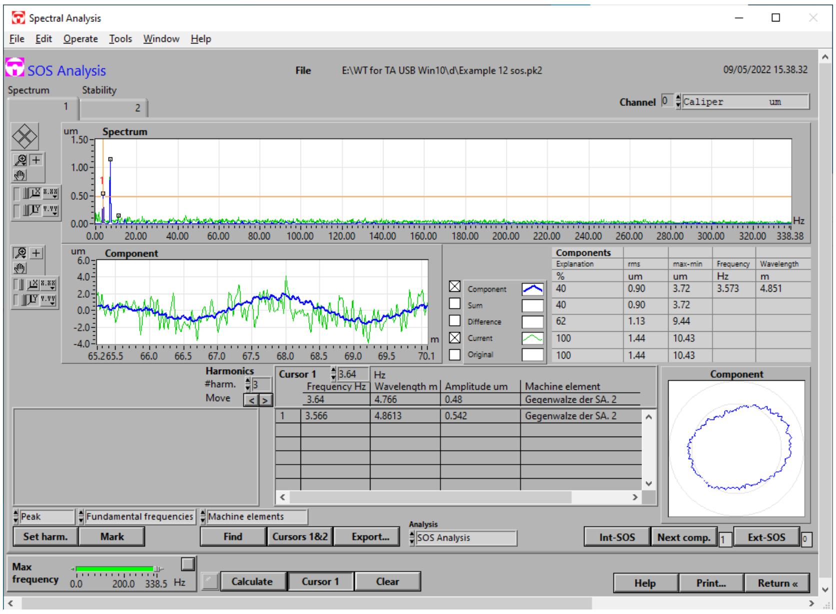

Figure 4.25: Tapio analyzer Spectral Analysis interface.

The signal used in this analysis is a caliper signal of 10992 samples, acquired with a sampling frequency of approximately 1300 Hz. The SOS extracts a frequency of 3.64 Hz which is close to 3.566 Hz, the frequency of a component in the machine. The optimal filter is applied with a frequency detection in the range $\pm 0.5\%\omega_0$, where ω_0 is equal to the frequency of the machine component, 3.566 Hz. The fundamental frequency detected by the optimal filter is equal to 3.560 Hz, which is closer than the one extracted by the SOS analysis to the frequency of the machine component. In this case, 30 harmonic components are extracted. Figure 4.26 shows the result for the two methods. The two extracted signals have similar behavior with the difference that the SOS signal also contains fluctuations at higher frequencies. Figure 4.27 reports on the left the amplitude values of the signal extracted by the filter with a fundamental frequency of 3.560 Hz, i.e. the one detected by the filter, and, on the right, the original caliper signal and the signal extracted by the filter in time.

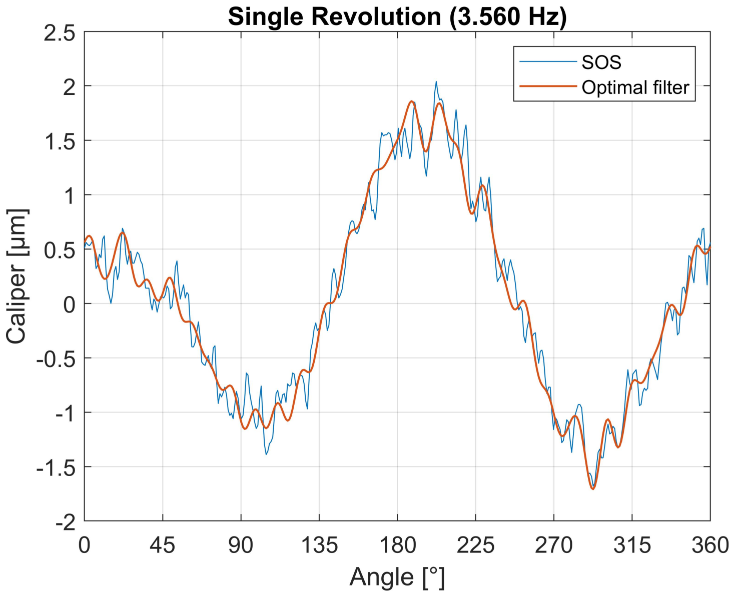

Figure 4.26: Comparison between the signal extracted by the SOS tool and the one extracted by the optimal filter.

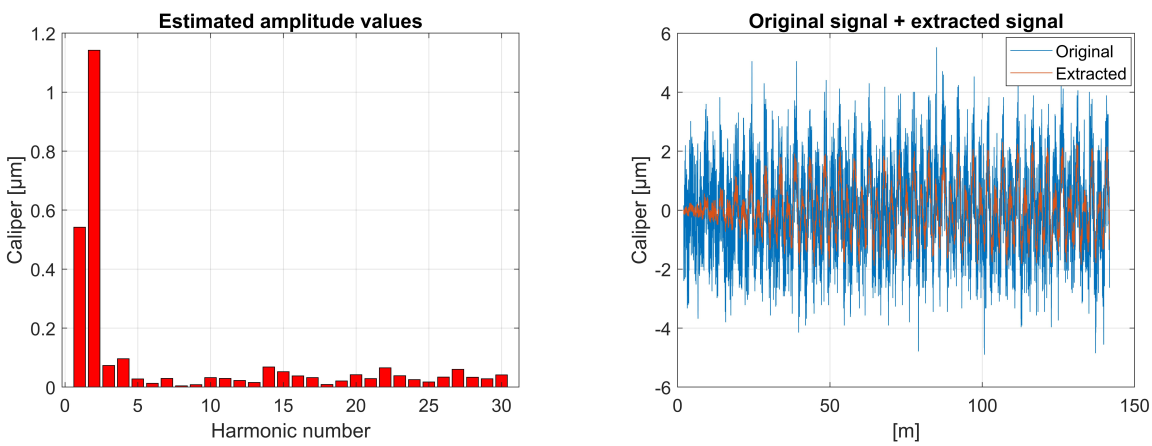

Figure 4.27: Amplitude values of the signal extracted by the filter (left). Original signal from the measurement and extracted signal in time (right).

5 | Discussion

The method demonstrated robust behavior in some non-ideal conditions. The results obtained on the artificially generated signal give an overview of the filter behavior in different situations and how to choose the filter parameters. Of course, the choice of parameters and the minimum level of acceptable performance must be chosen according to the application and the quality parameter under investigation.

The window length has been chosen in the performed tests to have at least an SDR of 4.5 for each roll. In the real application, the minimum acceptable value of SDR can be chosen by relating the error in the amplitude values of the harmonic components to the value of variation in the quality parameter that leads to the waste of the end product. The error, indeed, should be way smaller than the maximum acceptable value of quality variation. Moreover, the sampling frequency can be different from the one selected, depending on the available measurement setup. An additional factor to consider in choosing the number of samples in a real application is the stationarity of the signal. In fact, with a longer window, it is more probable that the signal shows a non-stationary behavior. This is important since the method does not handle well changes in frequency during the signal acquisition, as shown in the simulation with the chirp signal (Figure 4.16). Moreover, the window length affects the computational time. The latter depends on the system's computational power and can be subjected to some constraints that can make it necessary to shorten the window length. To decrease the overall computational time the calculation can be parallelized. Thanks to the parallelization, the effect of all rolls can be extracted at the same time, instead of done in sequence. This procedure reduces the time at the expense of the memory needed.

When the filter input frequency is absent from the signal, the amplitude of the harmonic components extracted by the filter is not null but similar to the noise level. However, this is not a big issue since it is reasonable to think that the RMS of the extracted signal is quite low. Since this analysis aims to identify the components causing most of the variation, those to which a high RMS of the output signal corresponds, the effect of the absent frequency has minor importance on the problem.

The possible mismatch between the input frequency, i.e. the set point of the rotational frequency, and the frequency of variation can be partly solved with the frequency detection. However, performing a frequency detection before extracting the filter result increases the computational time. In particular, the higher the resolution of the frequency detection the higher the computational time, but the more accurate the result. Moreover, the frequency range in which the detection is performed should be chosen considering the possible presence of similar frequencies.

As shown in the previous chapter, the filter is not always able to distinguish between two close frequencies. For example, with the parameter chosen in the tests reported in this thesis, the filter performance strongly decreases when the difference between two frequencies is around 0.02 Hz. Special caution should be exercised in the presence of such similar frequencies. A possible way to increase the filter resolution is to increase the number of samples N.

The method has proven to have good performances when applied to the synthetic signal but also when real data are used, even if in the last case it is not possible to quantitatively estimate the correctness of the results. Tests have been carried out on the synthetic signal to evaluate the applicability of the filter in the paper manufacturing process. Each application can require different values of the parameters, but the outcome of these tests can be used as a guide in their choice.

The method is proposed as a tool for condition monitoring of the machines. In fact, it makes it possible to assess the impact of each roll on the quality variation. This allows monitoring the roll's condition and detecting faults such as damage in the coating. Moreover, it can be used to identify errors in the geometry or excessive vibrations of rolls.

One positive aspect of this method is that it does not need additional offline measurement and it can make use of sensors already present in the machine. Additionally, the presented filter has some advantages compared to the classical usage of the Fourier transform. Mainly, it provides higher accuracy, and the choice of the input frequency is not limited by the frequency resolution.

6 Conclusion

This work analyzes a procedure for separating repeating patterns from machine direction quality variation. This can be used to monitor the condition of the machine and act on the component or machine section that causes the highest variations.

Firstly, a synthetic signal was generated to reproduce a signal of caliper variation measured on a paperboard sample. The signal was built as the sum of 9 harmonic series, reproducing the effect of 9 rolls in the machine, and noise. Different tests were performed modifying the signal to reproduce realistic situations that deviate from the ideal condition. The aim was to test the robustness of the method when some of the hypotheses of the filter were not satisfied. Subsequently, the filter was applied to available measured data from a production plant. Satisfying results were obtained in both cases, and the filter was finally validated through a comparison with a currently used software, showing an even better result.

When the 9 harmonic series were extracted from a signal with white noise and an SNR close to 1.5, the filter returned, in the worst case, a maximum average error in the amplitude values of the harmonic components of 0.014 µm. Moreover, the method compared to a software currently used in laboratory analysis showed a more accurate result. Indeed, the two methods showed similar results when extracting the effect of a machine component but the difference between the frequency extracted by the software and that of the machine component was 0.074 Hz, whereas it was only 0.006 Hz with the optimal filter.

This work represents the first study of the method, and it does not provide a ready-to-use tool for industries. Further research can be done to deepen and improve this study.

As a first improvement, a better understanding of the type and amplitude of noise present in the machine environment can help to generate an artificial signal that more closely reproduces the real one and better evaluate the results. Moreover, if the spectrum of the noise can be obtained, a pre-whitener can be applied before filtering. This would allow having a signal with white noise, thus respecting the hypothesis of the method.

To complete the study, additional tests should be done on real data acquired on the running machine. Data with a higher sampling frequency are needed. The sampling frequency of the available set of data was, in fact, too low to provide good results. Another interesting analysis might be to collect signals related to different quality parameters to understand which sections or components impact a particular parameter the most, under a nominal operating condition. For example, the press section can have a higher impact on basis weight.

Simulations in the production environment must be carried out to have practical feedback on the results and to modify the choice of parameters according to the outcome. An important factor to analyze in detail is the computational time. The latter must have a value that ensures effective monitoring so that action can be taken in a reasonable time if the quality level does not satisfy the target value. A further possible investigation consists in comparing the extracted harmonic series with known roll run out data to determine if they are correctly related. Finally, to improve the accuracy of the result, data should be acquired on different CD positions, deriving the outcome as an average of the results obtained for each position. In the present case, the probe of the sensor was held stationary in a single position.

Finally, in this work, the focus is on paper machines. Other manufacturing processes where the material is formed by rolls, such as steel and plastic film production, are not treated. The method should be reasonably applied, with some expedients, to these other processes as well.

Bibliography

[1] *Tissue World Magazine - Global average per capita tissue consumption stand at above 5Kg but 10Kg is possible.* https://www.tissueworldmagazine.com/departments/marketissues/global-average-per-capita-tissue-consumption-stands-at-above-5kg-but-10kg-is-possible/

[2] *Statista - Global paper packaging industry - statistics / facts.* https://www.statista.com/topics/9202/paper-packaging-industry-worldwide/#dossierKeyfigures

[3] *Knowpap - A learning environment for paper technology and factory automation* http://www.knowpap.com/extranet/suomi/knowpap_system/user_interfaces/knowpap.htm.

[4] Cutshall, K. *The nature of paper variation.* Tappi Journal, June 1990.

[5] Lehtiniemi, S. *Superresoluutiomenetelmä konesuuntaisen laatuvaihtelun analysointiin.* M.Sc. Thesis, Aalto University, Espoo, Finland, 2021.

[6] Rippon, Lee and Lu, Qiugang and Forbes, Michael and Gopaluni, Bhushan and Loewen, Philip and Backstrom, Johan. *Machine direction adaptive control on a paper machine.* Industrial & Engineering Chemistry Research, 2019. 58.26: 11452-11473.

[7] Christensen, M. *Introduction To Audio Processing,* Cham, Switzerland: Springer, 2019. ISBN 978-3-030-11780-1

[8] Christensen, M., Jakobsson, A. *Multi-Pitch Estimation,* Synthesis Lectures on Speech & Audio Processing, Morgan & Claypool, 2009. ISBN: 9781598298383

[9] Bertin, N., Badeau, R., Vincent, E. *Enforcing harmonicity and smoothness in Bayesian non-negative matrix factorization applied to polyphonic music transcription.* IEEE Transactions on Audio, Speech, and Language Processing, 2010, 18.3: 538-549.

[10] Mouyan, Z., Zhenming, C., Unbehauen, R. *Separation Of Periodic Signals By Using An Algenraic Method.* In: 1991 IEEE International Symposium on Circuits and Systems (ISCAS). IEEE, 1991. p. 2427-2430.

[11] Christensen, M., Jakobsson, A. *Optimal Filter Designs for Separating and Enhancing Periodic Signals.* IEEE Transactions on Signal Processing, 2010, 58.12: 5969-5983.

[12] Christensen, M., Jakobsson, A., Jensen, S. H. *Joint High-Resolution Fundamental Frequency and Order Estimation.* IEEE Transactions on Audio, Speech, and Language Processing, 2007, 15.5: 1635-1644.

[13] Maragos, P., Kaiser, J.F., Quatieri, T.F., *Energy separation in signal modulations with application to speech analysis.* IEEE transactions on signal processing, 1993, 41.10: 3024-3051.

[14] Hilden, K., Perento, J. *Paper analysis:the key to optimizing and troubleshooting paper machines.* Pulp & Paper Canada, 2000, 101.7: 37-42.

[15] Stoica, P., Li, H., Li, J. *A New Derivation of the Apes Filter.* IEEE Signal Processing Letters, 1999, 6.8: 205-206.

[16] Stoica, P., Moses R. *Spectral Analysis of Signals.* PRENTICE HALL, *Upper Saddle River, New Jersey 07458*, 2004. ISBN 0-13-113956-8

[17] Djuric, P. M. *Asymptotic MAP Criteria for Model Selection.* IEEE Transactions on Signal Processing, 1998, 46.10: 2726-2735.

[18] Christensen, M. *Accurate Estimation of Low Fundamental Frequencies from Real-Valued Measurements.* IEEE transactions on audio, speech, and language processing, 2013, 21.10: 2042-2056.

[19] Gerkmann, T., Hendriks, R.C. *Unbiased MMSE-Based Noise Power Estimation With Low Complexity and Low Tracking Delay.* IEEE Transactions on Audio, Speech, and Language Processing, 2011, 20.4: 1383-1393.

[20] Jaramillo, A.E., Nielsen, J.K., Christensen, M.G. *Adaptive Pre-whitening Based on Parametric NMF.* In: 2019 27th European Signal Processing Conference (EUSIPCO). IEEE, 2019. p. 1-5.

[21] Nørholm, S.M., Jensen, J.R., Christensen, M.G. *Instantaneous Fundamental Frequency Estimation with Optimal Segmentation for Non-Stationary Voiced Speech.* IEEE/ACM Transactions on Audio, Speech, and Language Processing, 2016, 24.12: 2354-2367.

[22] Särkkä, S. *Bayesian Filtering and Smoothing.* Cambridge University Press., 2013

[23] Waller, M.H. *On-line Papermaking Sensors: An Historical Perspective.* In The sci-

ence of papermaking, Trans. of the XIIth Fund. Res. Symp. Oxford, 2001, (C.F. Baker, ed.), pp 785–895, FRC, Manchester, 2018. DOI: 10.15376/frc.2001.2.785.

[24] Juhanko, J. *Dynamic geometry of a rotating paper machine roll.* Aalto University publication series, DOCTORAL DISSERTATIONS 117/2011.

[25] Tiainen, T., Viitala, R. *Effect of positional errors on the accuracy of multi-probe roundness measurement methods.* Mechanical Systems and Signal Processing, 2020, 144: 106883.

[26] Menon, A. *Methods and Tools Used in Paper Machine Supercalender Vibration Diagnostics.* In: Proceedings of 20th International Congress on Acoustics. Sydney: International Commission on Acoustics. 2010. p. 23-27.

[27] Juhanko, J., Väänänen, P. *Geometry of paper machine rolls.* Paper machine rolls seminar 27.-28.1.1999. Finnish Maintenance Society. Lahti.

[28] Kuosmanen, P. *Predictive 3D Roll Grinding Method for Reducing Paper Quality Variations in Coating Machines.* Helsinki University of Technology Publications in Machine Design 2/2004.

[29] Choudhury, T., Viitala, R., Kurvinen, E., Raine Viitala, R., and Sopanen, J. *Unbalance Estimation for a Large Flexible Rotor Using Force and Displacement Minimization.* Machines, 2020, 8.3: 39.

[30] Viitala, R., Tiainen, T., and Viitala, R. *Effect of Rotor Geometry on Bending Stiffness Variation.* Machines, 2021, 9.2: 23.

[31] Viitala, R. *Effect of Assembled Bearing Inner Ring Geometry on Subcritical Rotor Vibration.* Aalto University publication series, DOCTORAL DISSERTATIONS 183/2018.

[32] Widmaier, T. *Optimisation of the roll geometry for production conditions.* Doctoral dissertation. Aalto University, Espoo. ISBN 978-952-60-4879-6 (2012).

[33] Viitala, R., Widmaier, T., and Kuosmanen, P. *Subcritical vibrations of a large flexible rotor efficiently reduced by modifying the bearing inner ring roundness profile.* Mechanical Systems and Signal Processing, 2018, 110: 42-58.
`https://doi.org/10.1016/j.ymssp.2018.03.010`.

[34] *Valmet website*
`https://www.valmet.com`

[35] *Tapio Technologies website*
https://tapiotechnologies.com

[36] ISO 21940-12, 2016. Mechanical vibration. Rotor balancing. Part 12: Procedures and tolerances for rotors with flexible behaviour. www.iso.org

[37] ISO 1101, 2017. Geometrical Product Specifications (GPS). Geometrical tolerancing – Tolerances of form, orientation, location and run-out. www.iso.org

[38] ISO 12181-1, 2011. Geometrical product specifications (GPS) – Roundness – Part 1: Vocabulary and parameters of roundness. www.iso.org

[39] ISO 12181-2, 2011. Geometrical product specifications (GPS) – Roundness – Part 2: Specification operators. www.iso.org

A | Appendix A

A.1. Rotational frequencies of the rolls in the paper machine.

Table A.1: List of known rotating frequencies of rolls in the machine used in the data acquisition.

Roll n.	Frequency [Hz]	Diameter [m]
1	2.080	1.531
2	2.085	1.528
3	2.088	1.525
4	2.090	1.524
5	2.090	1.524
6	2.121	1.501
7	2.352	1.354
8	2.439	1.306
9	2.553	1.247
10	2.727	1.168
11	2.805	1.135
12	2.964	1.074
13	3.047	1.045
14	3.097	1.029
15	3.154	1.010
16	3.158	1.008

Continued on next page

Table A.1: List of known rotating frequencies of rolls in the machine used in the data acquisition. (Continued)

Roll n.	Frequency [Hz]	Diameter [m]
17	3.250	0.980
18	3.280	0.971
19	3.333	0.955
20	3.730	0.854
21	4.272	0.745
22	4.539	0.702
23	6.342	0.502
24	7.048	0.452
25	7.054	0.451
26	7.059	0.451
27	7.070	0.450
28	7.074	0.450
29	7.076	0.450
30	7.077	0.450
31	7.160	0.445
32	7.486	0.425
33	7.875	0.404
34	8.246	0.386
35	8.585	0.371
36	11.430	0.279
37	14.016	0.227
38	14.112	0.226

List of Figures

List of Tables

List of Symbols and Abbreviations

Symbols

Δf	frequency resolution
f_s	sampling frequency
N	signal length
ω_k	fundamental frequency of the kth source
$\mathbf{R}$	signal covariance matrix
$\mathbf{Q}$	noise covariance matrix
k	source index
l	harmonic component
L_k	model order for the kth harmonic series
A	amplitude value
ϕ	phase
x	signal
e	noise
y	filtered signal
$\mathbf{h}$	vector of filter coefficients
$\mathbf{P}$	amplitudes covariance matrix
$\mathbf{a}$	amplitudes vector
$\mathbf{Z}$	Vandermonde matrix
$\mathbf{x}$	vector of signal samples
M	filter length
$\hat{\mathbf{R}}$	estimated signal covariance matrix
$\hat{\mathbf{Q}}$	modified covariance matrix
$\hat{y}$	desired output

Operators

$E\{x\}$	expected value
x^T	transpose operator
x^H	hermitian operator

Abbreviations

MD	machine direction
CD	cross direction
R	random or residual variation
DFT	discrete Fourier transform
FFT	fast Fourier transform
RMS	root mean square error
SOS	separate original signal
APES	amplitude and phase estimation
SNR	signal to noise ratio
SIR	signal to interference ratio
QCS	quality control system
MSE	mean square error
PSD	power spectral density
ISO	International organization for standardization
BSV	bending stiffness variation
SDR	signal to distortion ratio

Acknowledgements

I would like to thank Raine Viitala for allowing me to work in his research group and Aalto University and Politecnico di Milano for allowing me to carry out this semester in Finland as an exchange student. Moreover, I want to thank Tuomas Tiainen for his excellent guidance and the rest of the ARotor research team. Finally, I want to thank Professor Marco Tarabini from Politecnico di Milano for his support.